THE KINEMATICS OF WATER PARTICLE VELOCITIES OF BREAKING WAVES WITHIN THE SURF ZONE

David Paul Richardson

THESIS

THE KINEMATICS OF WATER PARTICLE VELOCITIES OF BREAKING WAVES WITHIN THE SURF ZONE

by

David Paul Richardson

Thesis Advisor: E.B. Thornton

September 1973

The Kinematics of Water Particle Velocities of Breaking Waves Within the Surf Zone

by

David Paul Richardson
Lieutenant Commander, United States Navy
B.S., B.A., University of Missouri, 1963

Submitted in partial fulfillment of the
requirements for the degree of

MASTER OF SCIENCE IN OCEANOGRAPHY

from the

NAVAL POSTGRADUATE SCHOOL
September 1973

ABSTRACT

Simultaneous measurements of waves, and vertical and horizontal water particle velocities were made at the breaker-line within the surf zone using a capacitance type penetrating wave staff, a pressure wave gauge, and an electromagnetic current meter. Wave measurements were also made at seaward and shoreward locations. The wave energy-density spectral components were converted to velocity spectral components using linear wave theory. These computed values compared well qualitatively with the measured velocity spectra. Quantitatively, the results showed that linear theory underpredicted wave-induced horizontal velocity spectral components by about 50 percent at the frequency of peak energy. The coherence values between waves and horizontal velocity were high, ranging above 0.75. The phase angle computation showed the calculated velocity components leading the measured velocity components by an average of 20 degrees, indicating an unstable wave crest leading the particle motion in the body of the wave. Probability density functions were computed and compared to Gaussian and Gram-Charlier distributions using the chi-square goodness-of-fit test. The Gram-Charlier distribution qualitatively gave the better fit to the data.

TABLE OF CONTENTS

LIST OF TABLES

LIST OF FIGURES

I. INTRODUCTION

A. NATURE OF THE PROBLEM

The problem is to describe the kinematics of breaking waves within the surf zone in terms of the water surface elevation. The theories which have been developed for deep water waves can be applied with some degree of certainty, and can be tested in a laboratory situation. These theories generally hold up to the time that the wave begins to shoal, and with somewhat lesser accuracy, throughout the shoaling process up to the point of breaking. At the breaker point, however, the prediction of wave kinematics becomes more difficult. The type of breaking wave, plunging, surging, or spilling, depends upon deep water characteristics, bottom type, and bottom slope, hence requiring a different description of the kinematics within the wave for each breaker type. Physical limitations preclude the construction of a realistic laboratory model of the surf zone. And finally, the hostile character of the surf zone complicates the taking of *in situ* measurements to the degree that relatively little data exist from within the surf zone.

The most forthright approach to the problem of describing the kinematics of breaking waves in the surf zone seems to be through direct measurements. Advances in instrument design have led to simple, sturdy, measuring devices with rapid response time which can sense the small scale as well as the large scale features. By making the assumption that

the processes are stationary, this assumption being valid at least over a short record of 20 to 30 minutes, the waves and wave induced particle velocities can be dealt with as stationary random phenomena, thereby allowing the utilization of standard statistical analysis procedures.

B. REVIEW OF PREVIOUS WORKS

The study of the kinematics of breaking waves in the surf zone has progressed slowly both due to the difficulty in making direct field measurements, and due to the difficulty in modeling the surf zone in the laboratory.

Early work by Iversen (1953) involved use of a wave channel in which waves were generated using a hinged plane oscillating flap. Measurements were made using photographic techniques. The length of the channel limited the wave type to plunging and surging breakers. Adeyemo (1970) made similar laboratory measurements using hydrogen bubble and photographic methods.

Inman (1956) made field measurements of water particle velocity by measuring the drag force under the wave in order to infer particle velocities. Miller and Zeigler (1964) used both acoustic and electromagnetic current meters to determine the particle motion in the surf zone. Walker (1969) made studies using propeller type flow meters. Thornton (1968) and Steer (1972) made use of electromagnetic current meters to measure the particle motion.

C. OBJECTIVE

The objective of this research is to study the kinematics of water particles in breaking waves within the surf zone. Simultaneous measurements were made of the instantaneous water surface elevation and two orthogonal water particle velocities at a fixed location in the surf zone. Additional wave measurements were made at points seaward and shoreward of the primary location. Estimates of the probability density functions and power spectra of the wave height and particle velocities are to be made. The applicability of linear wave theory is to be measured in computing velocity spectral components using the energy-density spectrum of the waves. The computed velocity spectra are to be compared with actually measured velocity spectra.

II. STATISTICAL ANALYSIS

It was assumed that the data to be analyzed represents realizations of stationary, random processes. This assumption allows the use of standard statistical techniques. The basic analyses are described in the following sections as if performed on continuous data of infinite duration for ease of discussion. The actual analyses were performed digitally on records of finite length.

A. PROBABILITY DENSITY FUNCTION

The probability density function describes the probability that a sample time history record $x(t)$ will assume a value between x and $(x + \Delta x)$, and that this approaches an exact probability as T, the observation time, approaches infinity, and as the defined range, Δx, approaches zero. The probability density function is given mathematically as:

$$P(x) = \lim_{\Delta x \to 0} \lim_{T \to \infty} \frac{1}{\Delta x} \frac{T_i}{T} \qquad (2.1)$$

Where T_i is the amount of time that $x(t)$ falls within the range $(x, x + \Delta x)$.

The computed probability density function was compared to the Gaussian and Gram-Charlier distributions and tested for comparison using the chi-square goodness-of-fit test.

The Gaussian probability density function is given as:

$$P_{Ga}(x) = \frac{1}{\sigma \sqrt{2\pi}} e^{-(x-\mu)^2/2\sigma^2} \qquad (2.2)$$

where σ = standard deviation

μ = mean

and in standardized form, with $z = \frac{x-\mu}{\sigma}$,

$$P_{Ga}(z) = \frac{1}{\sqrt{2\pi}} e^{-z^2/2}$$

The Gaussian distribution is completely described by the mean and variance, and has zero skewness and kurtosis equal to three.

The Gram-Charlier distribution was shown by Longuet-Higgins (1963) to better describe the probability distribution of the instantaneous water surface elevation, $\bar{\eta}$, in moderately non-linear swell in deep water. It is given by:

$$P_{Gc}(z) = P_{Ga}(z)[1.0 + \frac{m_3}{24} H_3 + (\frac{m_4}{24} H_4 + \frac{m_3^2}{72} H_6) + \ldots] \qquad (2.3)$$

where

$$H_n = z^n - \frac{n(n-1)}{1!} \frac{z^{n-2}}{2} + \frac{n(n-1)(n-2)(n-3)}{2!} \frac{z^{n-4}}{2^2}$$

(Hermite Polynomial)

m_3 = skewness of record

m_4 = kurtosis - 3

It can be seen that for zero skewness and kurtosis of three, the fourth order Gram-Charlier distribution degenerates to the Gaussian distribution.

To apply the chi-square goodness-of-fit test, the random variable, x(t), was divided into K intervals, called class intervals, thereby forming a frequency histogram. The observed frequency, f_i, is the number of observations within the ith class interval. The expected frequency, F_i, is the number of observations which fall in the ith interval of the theoretical distribution. The total discrepancy between the observed and expected frequency is given by:

$$\chi^2 = \sum_{i=1}^{K} \frac{(f_i - F_i)^2}{F_i} \qquad (2.4)$$

As the value of χ^2 increases from zero, the goodness-of-fit decreases.

B. SPECTRAL ANALYSIS

1. Energy-Density Spectrum

The auto-covariance for a record, x(t), is defined mathematically by

$$R_{11}(\tau) = \lim_{T\to\infty} \frac{1}{T} \int_{t}^{t+T} x_1(t)x_1(t+\tau)dt \qquad (2.5)$$

The value obtained describes the dependence of the values of the data set at one point in time on the values at some later time, τ, in the data set. The function is real-valued and

even, and has a maximum at $\tau = 0$. The above expression implies an infinitely long data set. To deal with the reality of a data set of finite length, a lag window is applied. The choice of lag window for this analysis was the Parzen lag window, because it has the advantage of no negative side lobes, which maintains the coherence function between its theoretical values of ± 1. It also insures no numerical resonance problems when computing cross-spectra. The Parzen window is given by Bendat and Piersol (1966) as:

$$P(\tau) = \begin{cases} 1 - 6\left(\frac{\tau}{T_m}\right)^2 + 6\left(\frac{\tau}{T_m}\right)^3 & , \quad \tau = 0,1,2,\ldots,\frac{T_m}{2} \\ 2\left[1 - \frac{\tau}{T_m}\right]^3 & , \quad \tau = \frac{T_m}{2} + 1,\ldots,T_m \\ 0 & , \quad \tau > T_m \end{cases} \tag{2.6}$$

The energy-density spectrum is computed from the Fourier transform of the covariance function as modified by the Parzen lag window. The spectrum is given by:

$$S_{11}(f) = \int_{-\infty}^{\infty} P(\tau) R_{11}(\tau) e^{-i2\pi f\tau} d\tau \tag{2.7}$$

where f is a particular frequency of interest.

2. Cross-Spectral Density

The cross-covariance function describes the general dependence of the values of one set of data on the other set, in contrast to the auto-covariance function which compares a

record against itself. The cross-covariance function is given mathematically as:

$$R_{12}(\tau) = \lim_{T\to\infty} \frac{1}{T} \int_{t}^{t+T} x_1(t)x_2(t+\tau)dt \qquad (2.8)$$

The quantity $R_{12}(\tau)$ is a real-valued function, but it is not an even function, and does not necessarily have a maximum value at $\tau = 0$.

A lag window again is applied to the cross-covariance function before computing the cross-spectral density. Applying the Parzen window and taking the Fourier transform, the cross-spectral density is given by:

$$S_{12}(f) = \int_{-\infty}^{\infty} P(\tau)R_{12}(\tau)e^{-i2\pi f\tau}d\tau \qquad (2.9)$$

Since, unlike the energy-density spectrum, the cross-spectrum is not an even function, it is expressed in real and imaginary parts by:

$$S_{12}(f) = C_{12}(f) - i\, Q_{12}(f) \qquad (2.10)$$

The real part, called the co-spectrum, is given by:

$$C_{12}(f) = 2 \int_{0}^{\infty} P(\tau)[R_{12}(\tau) + R_{12}(-\tau)]\cos(2\pi f\tau)d\tau \qquad (2.11)$$

The imaginary part, called the quadrature spectrum, is given by:

$$Q_{12}(f) = 2 \int_{0}^{\infty} P(\tau)[R_{12}(\tau) + R_{12}(-\tau)]\sin(2\pi f\tau)d\tau \qquad (2.12)$$

3. Phase Angle

Equation (2.10) can be rewritten in complex polar notation in terms of the modulus of the cross-spectral density and a phase angle,

$$S_{12}(f) = |S_{12}(f)|e^{-i\varepsilon_{12}(f)} \tag{2.13}$$

where $\varepsilon_{12}(f)$ = average angular difference by which the cross-correlated components of $x_2(t)$ lead those of $x_1(t)$ in each spectral band. The phase angle expressed in terms of the co-spectra and quadrature-spectra is given by:

$$\varepsilon_{12}(f) = \tan^{-1}\left[\frac{Q_{12}(f)}{C_{12}(f)}\right] \tag{2.14}$$

where

$$-\pi \leq \varepsilon_{12}(f) \leq \pi$$

4. Coherence

An expression for the comparison of two random variables as a function of frequency is described by the coherency squared, or simply coherence, and is derived using the expressions previously stated for energy-density spectra and for cross-spectral density. In mathematical terms, the coherence function is given as:

$$\gamma_{12}^{2}(f) = \frac{|S_{12}(f)|^2}{S_{11}(f)S_{22}(f)} \tag{2.15}$$

where:

$$0 \leq \gamma_{12}^{2} \leq 1$$

The coherence function has the characteristics that when $\gamma_{12}^2(f) = 1$, the two records are completely correlated at that frequency; and when $\gamma_{12}^2(f) = 0$, the records are statistically independent at that frequency.

III. EXPERIMENTAL PROCEDURE

A. EXPERIMENTAL SITE

The experiment was conducted at Del Monte Beach inside Monterey Bay adjacent to Monterey, California, on 12 April, 1973. The beach profile shown in Figure (1) is one of gentle slope. Plunging and spilling breakers are very common at this site, with spilling breakers being the predominant type. The waves at this location are usually severely directionally filtered by refraction due to the geometry of the coastline and bay, and approach almost perpendicular to the shore.

B. INSTRUMENTATION

The primary measuring instruments were placed on a three meter steel tower as shown in Figure (2). The tower was guyed so that tower movement and vibration were negligible. The instruments were arranged so as to be in the same vertical plane, with the exception of a small offset parallel to the wave crests given to the water current meter to prevent interaction with the capacitance probe.

The water particle velocities were measured with an Engineering Physics Company water current meter Model 6130. The sea surface elevation was measured with a capacitance type penetrating wave staff fabricated locally, and with an Interstate Electronics Model DP-200 portable wave recorder with SDP-201 differential pressure sensor.

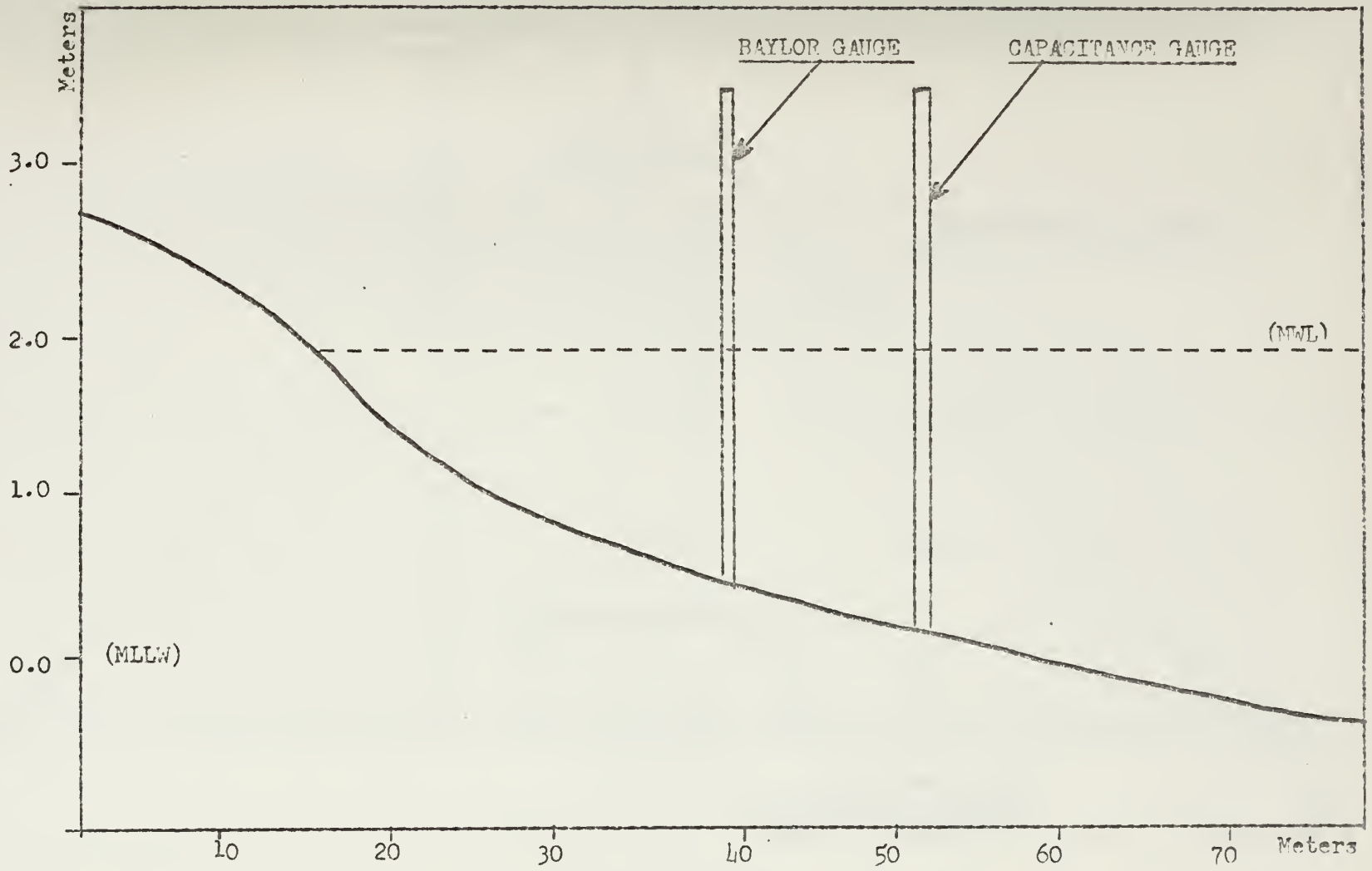

FIGURE 1. Beach Profile at Experimental Site

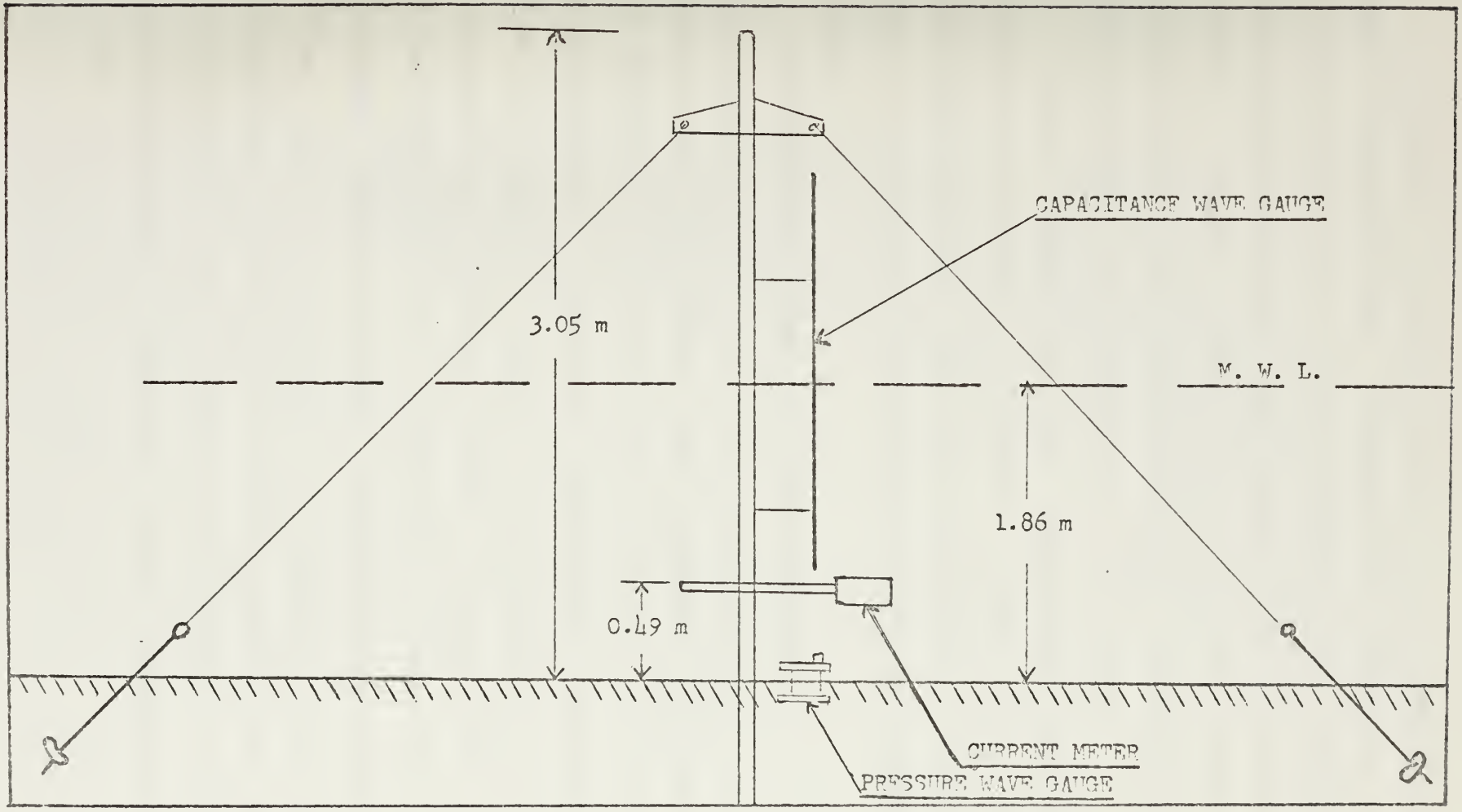

FIGURE 2. Schematic of Main Instrument Tower

Additional instrumentation was placed seaward and shoreward of the main tower. A pressure wave gauge was installed seaward of the main tower by mounting it on a weighted sled. The sled was towed into position by attaching a winch cable from R. V. Acania. Acania, in her anchored position, heaved around, pulling the sled into position. The mean water at the sled during the experiment was 2.69 meters.

A Baylor Company Wave Staff System Model 13528R was installed 12.9 meters shoreward on a steel tower. This wave staff was placed in a line with the primary tower and the sled so as to be on an orthogonal with the predicted wave crests.

The capacitance wave staff was designed by L. F. McGoldrick (1969) at the University of Chicago as an inexpensive, but ultra-linear highly sensitive instrument for the detection of capillary waves in the 20 to 30 HZ range. It operates on the principal that changing the plate dimensions of a capacitor changes its capacitance and hence its influence on an electrical circuit. The probe was constructed of one-eighth inch O. D. bronze wire; a dialectric of one-sixteenth inch wall thickness polystyrene tubing which fitted tightly over the wire; and appropriate electrical connections. The sea water in which the probe was immersed constituted the second plate of the capacitor. The probe was held stationary on the tower, and as the sea level fluctuated, the capacitance changed accordingly. These fluctuations were sensed by a transistorized circuit operated by

two self-contained ten volt batteries. The electronics section was housed in a watertight case which was mounted on the tower. This enabled the connecting leads to be relatively short, thereby minimizing wire-to-wire capacitance. A static calibration of the system was made by immersing the staff in a water tank. The resulting calibration is shown in Figure (3).

The Interstate Electronics Pressure Sensor used on the primary tower and at the sled site is a small, unbonded strain gauge bridge. The sea pressure is coupled by a neoprene diaphragm to a silicone fluid filling the interior. The arrangement is such that slow changes, such as tides, are lost through the hydraulic filter, and the transducer only senses the rapid pressure fluctuations of waves. The high-pass filter response time constant is 48 seconds.

The Engineering Physics Company electromagnetic current meter measures two orthogonal components of water particle velocity through a range of zero to one and one-half M/SEC with a maximum output error of one percent of full scale reading. The instrument has two electrical time constant settings, 0.3 and 1.0 seconds. The operation of the unit is based on Faraday's principle of magnetic induction. Faraday discovered that currents are induced in a conductor which is put in motion through a magnetic field. This induction can be expressed by the vector equation:

$$\vec{E} = \vec{U} \times \vec{B}$$

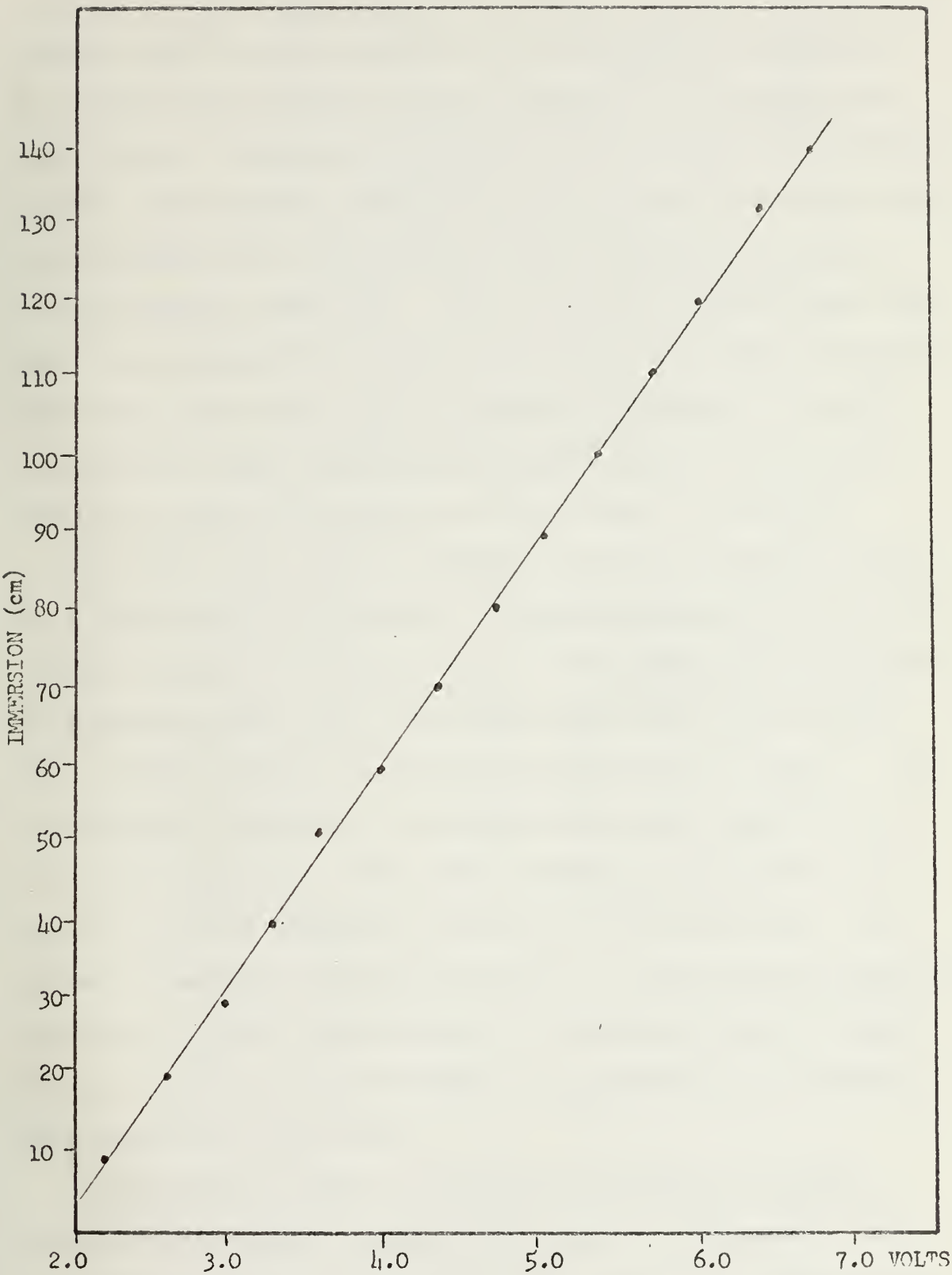

FIGURE 3. Capacitance Wave Staff Calibration Curve

where $\vec{E}$ is the induced electric field, $\vec{U}$ is the velocity of motion, and $\vec{B}$ is the intensity of the magnetic induction. In the sea the induced electric field, $\vec{E}$, is linearly proportional to the amount of fluid flowing through the magnetic field. The magnetic field, $\vec{B}$, is most intense near the probe, and decreases with the distance from the probe according to the inverse square law. Thus, the flow velocity near the probe is weighted more heavily than that away from the probe, with only that water which is within a distance of two to three probe radii contributing significantly to the flow induced voltage. The radius of the probe is 3/8 inch.

The flow meter was recalibrated using the method of Krapohl (1972) and Steer (1972). This procedure involves oscillating the probe in a water tank. The equipment arrangement is shown in Figure (4). The flow meter probe was mounted on a carriage which travelled back and forth on rails. The carriage was driven by a variable speed motor geared to an eccentric throw arm. The peak carriage velocity was calculated to be the tangential velocity of the throw arm. The values of maximum carriage velocity, V_t, and maximum measured velocity, V_m, were determined for different angular frequencies. Each pair of electrodes was calibrated by orienting them parallel to the flow.

Figure (5) is a plot of the ratio of measured maximum velocity and maximum carriage velocity vs. frequency. The instrument's response is shown to be flat out to frequencies of about 0.5 Hz. At higher frequencies, the cart became

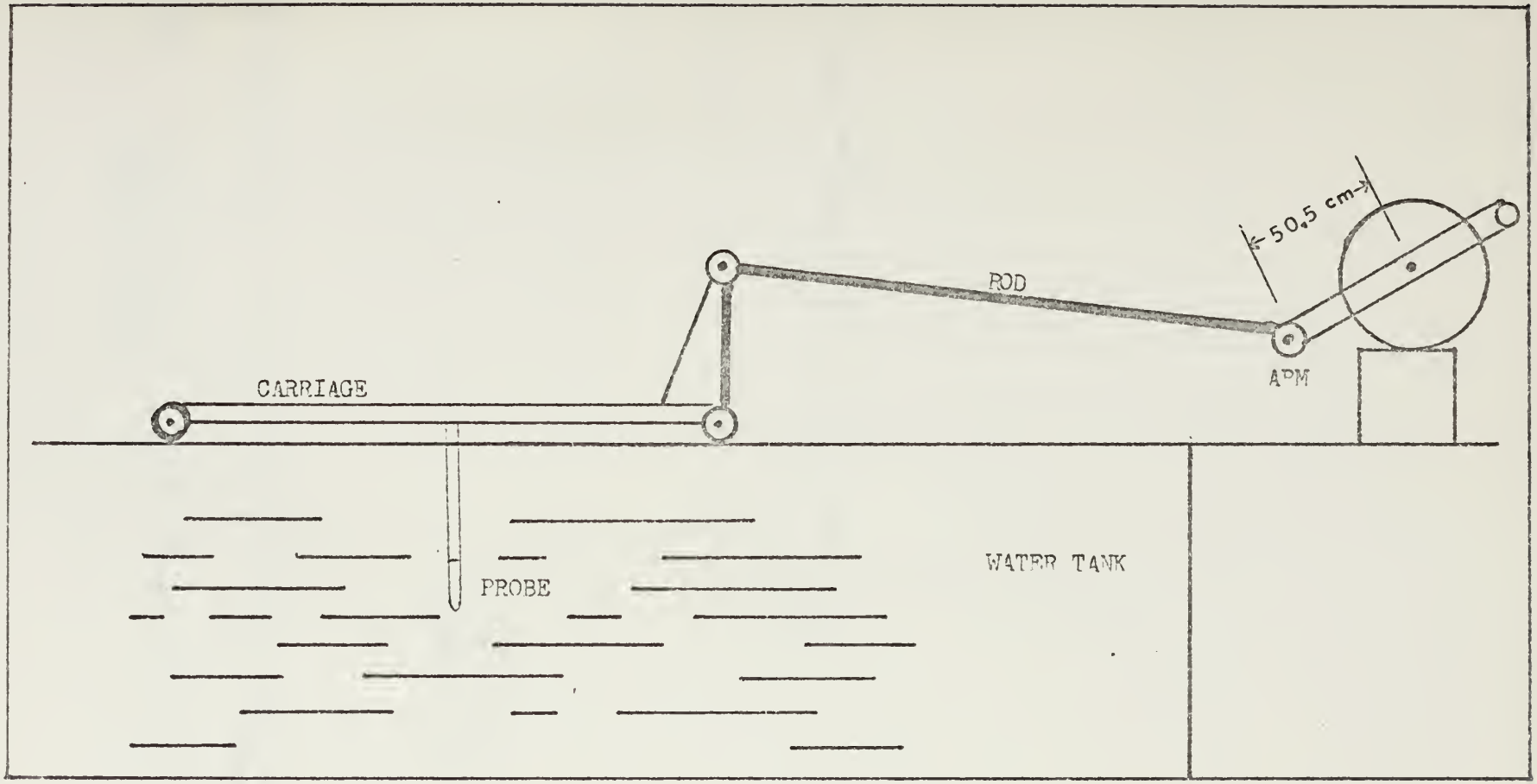

FIGURE 4. Electromagnetic Current Meter Calibration Assembly

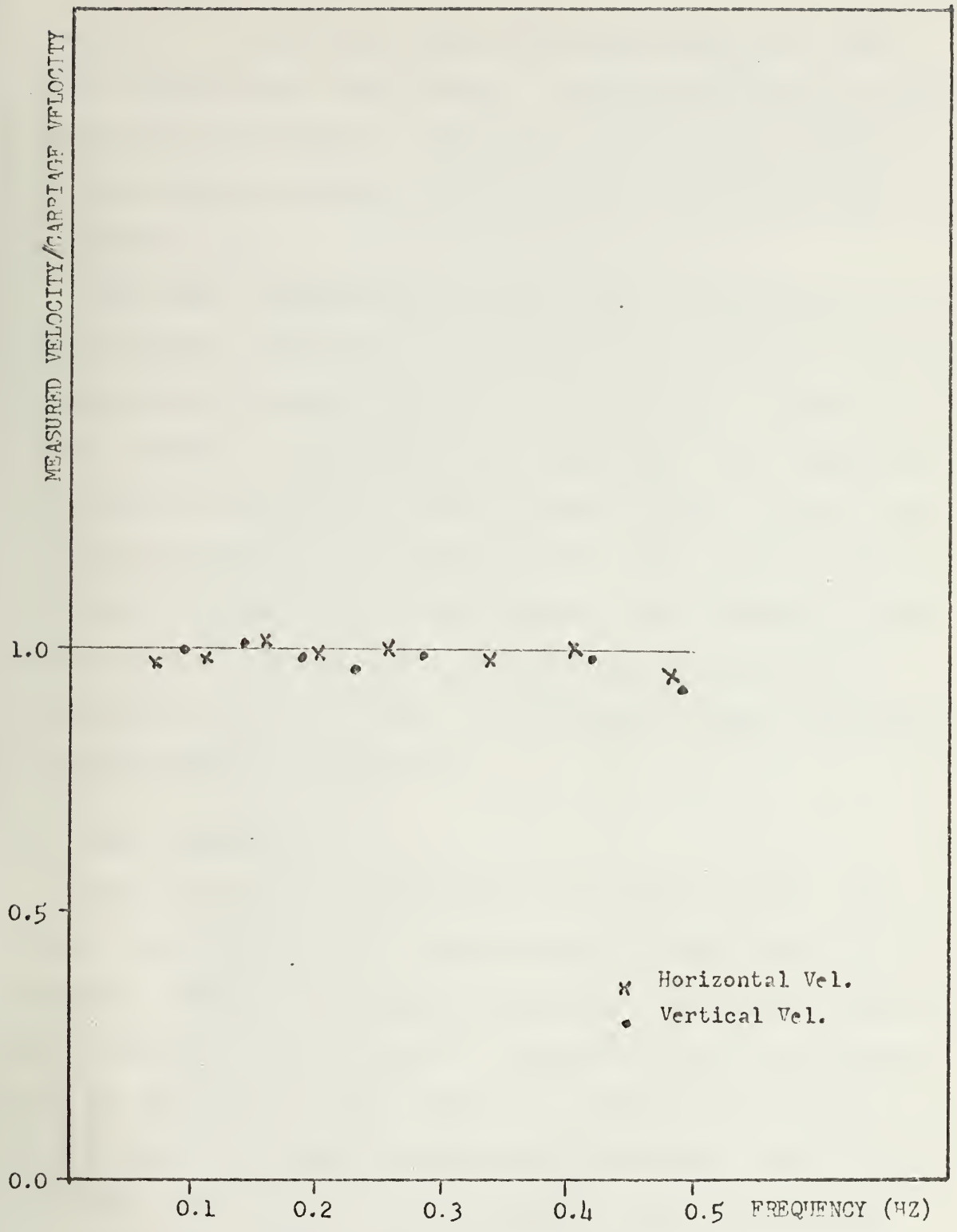

FIGURE 5. Electromagnetic Current Meter Frequency Response Curve

unstable. In addition, waves were generated in the tank which affected the flow pattern. This upper frequency limitation was not deemed a significant factor in measurement of ocean waves in which the significant energy was found to be below 0.5 Hz.

The Model 13529R Baylor Company Wave Staff System is an instantaneous water level measuring device consisting of two tensional half inch, 6x19 IWRC SS wire ropes. Together with these lengths of stainless steel wire rope, the transducer produces an electrically linear direct current output that is proportional to the amount of wave staff above a short circuit produced by the water surface. The working length of the staff, through previous modifications, had been shortened from 50 to 5 feet. The results of the recalibration are shown in Figure (6).

C. DATA COLLECTION

The experiment was performed on 12 April, 1973. The towers and sled had been installed at low tide two days previously. Tests were conducted and final calibration checks were made on 11 and 12 April. Included in the calibration was the placing of a two volt D. C. reference voltage on the FM tape to be used during data processing. This insured that the signal gains could be checked after digitizing.

During the afternoon of 12 April, swell from a storm off the Washington coast began to arrive, with a buildup to peak wave height coincident with high tide. During the experiment,

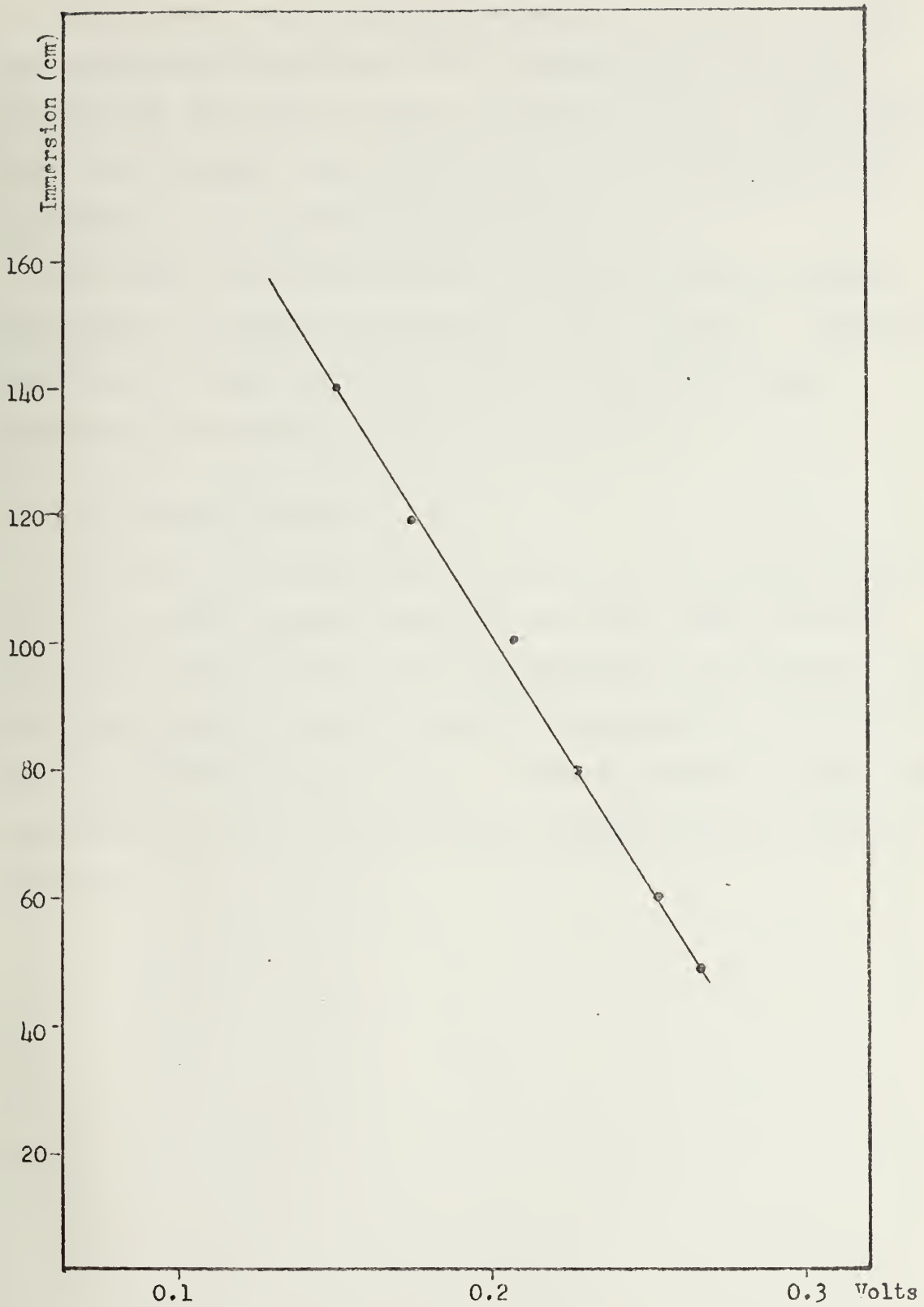

FIGURE 6. Baylor Wave Gauge Calibration Curve

the significant wave height at breaking was about 1 meter. The waves were generally of the plunging type, and were breaking in the general area of the main tower. The breaker point was visually observed to move seaward and shoreward according to the incident wave height.

All data were simultaneously recorded using a Sangamo Model 3500, 14 channel FM magnetic tape recorder. Continuous monitoring of data was accomplished using strip chart recorders and voltmeters.

D. DATA PRE-PROCESSING

The data were transcribed using the CS-500 Analog Computer to an eight channel Clevit Brush strip chart recorder for signal verification. It was digitized and recorded onto seven track tape using the XDS-9300 computer in conjunction with the CS-500 Analog Computer. The digitized records were transferred to nine track tape for analysis by the IBM 360 computer.

IV. ANALYSIS OF DATA

Figures (7) and (8) are typical records showing that the breaking waves were roughly triangular in shape and were very peaked. This corresponds to the general observation that plunging breakers at or near the breaker point have a steep, almost vertical front face, and a sloping profile toward their trailing edge. The records show small peaks between the primary wave peaks. It is thought that the small peaks are harmonics of the primary wave frequency.

The capacitance gauge showed a more sharply peaked wave than did the pressure gauges. This was due to the nature of the instruments in that the capacitance gauge could sense more rapid changes in the wave slope.

A. SAMPLING PROCEDURE

The data were read at a rate of 3 samples per second, corresponding to a sample interval of 0.33 seconds. This resulted in a Nyquist frequency of 1.5 Hz. The sampling rate was considered to be sufficiently high to avoid aliasing of energy into the portion of the spectra which was of interest from observations of the analog record.

The length of record analyzed was 21 minutes. The maximum lag time was taken as five percent of the record giving a spectral bandwidth resolution of 0.00873 Hz. According to Blackman and Tukey (1958), this yields 40 degrees of freedom. By applying the chi-square distribution, the 80 percent

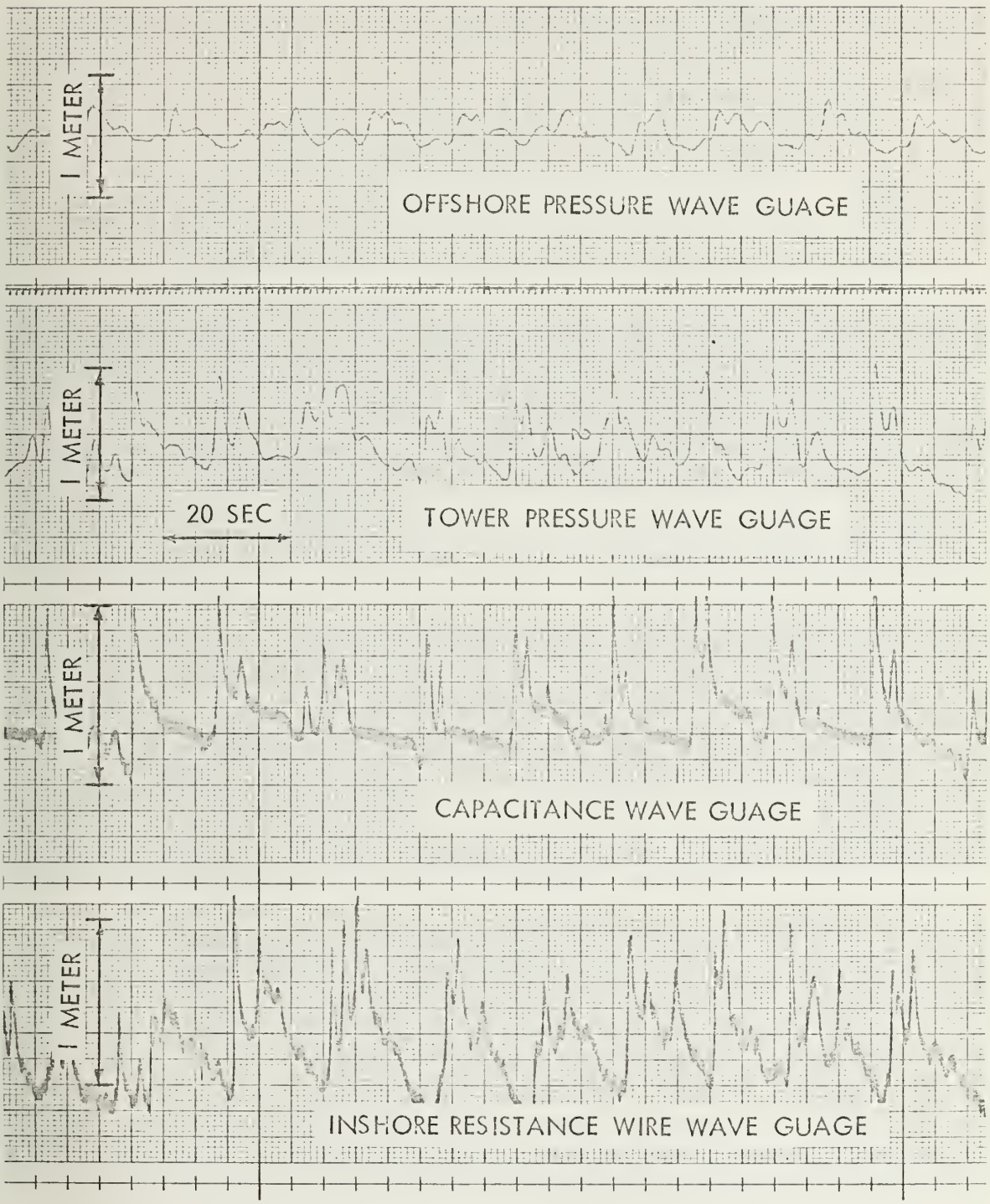

FIGURE 7. Strip Chart Record of Waves

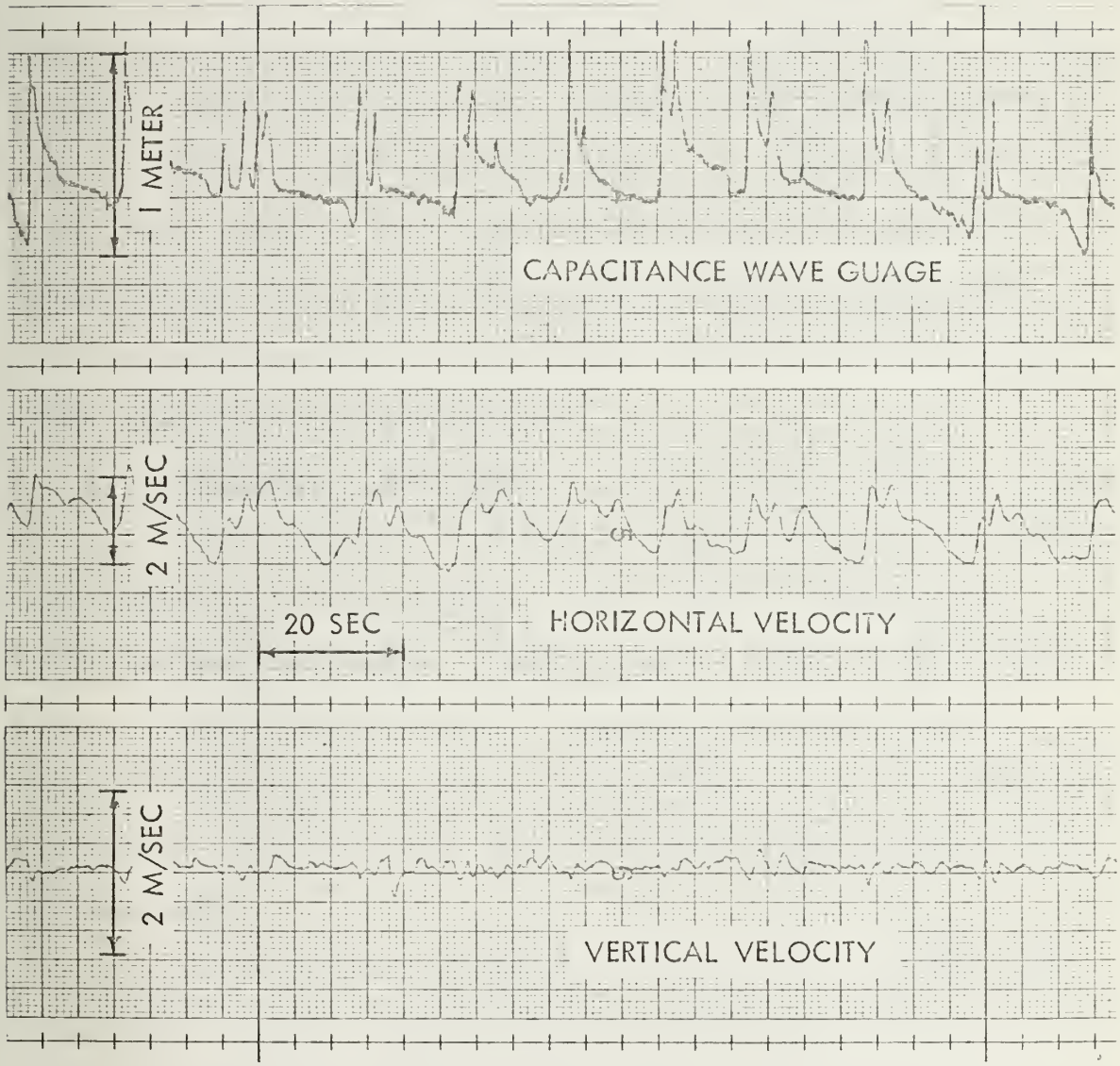

FIGURE 8. Strip Chart Record of Waves and Particle Velocities

confidence limits for 40 degrees of freedom are found to be between 0.77 and 1.38 of the measured power spectral estimates.

B. PROBABILITY DENSITY FUNCTION

The probability density function, pdf, for each wave and water particle velocity record was estimated using the procedures outlined in Section II-A. For each record, the standard deviation, variance, skewness, and kurtosis were computed and are summarized in Table I. Measured distributions were compared with the Gaussian and Gram-Charlier distributions using the chi-square goodness-of-fit test. The various measured distributions were also plotted against these analytical distributions.

1. Sea Surface Elevation

At the seaward station, the measured wave pdf shows some relation to the Gaussian distribution [Figure(9)]. The Gram-Charlier gives a better fit in terms of the chi-square goodness-of-fit test. This is to be expected in that the Gram-Charlier pdf is calculated using the assigned parameters from the data, and including moments higher than the second.

At the primary station, the pdf again follows the Gram-Charlier more closely than the Gaussian, but not to as great a degree as in the deeper water case [Figures (10) and (11)].

TABLE I

SUMMARY OF PROBABILITY DENSITY FUNCTION COMPUTATIONS

	MEAN	VARIANCE	STD. DEV.	P.D.F. SKEWNESS	P.D.F. KURTOSIS	χ^2 (Gauss.)	χ^2 (Gram-Char)
Outer Pressure Wave Gauge		0.0144 m^2	0.1201 m	0.6436	3.5679	332.8	76.9
Main Pressure Wave Gauge		0.0493 m^2	0.2220 m	0.6251	3.0797	464.7	162.4
Capacitance Wave Gauge	1.86 m	0.0304 m^2	0.1745 m	1.1304	4.4842	93.2	43.0
Baylor Wave Gauge	1.90 m	0.0745 m^2	0.2729 m	0.3294	2.8154	172.2	78.9
Horizontal Current Meter	0.2093 m/sec	0.2918 $(m/sec)^2$	0.5402 m/sec	0.2021	2.5382	146.4	72.4
Vertical Current Meter	0.0812 m/sec	0.0078 $(m/sec)^2$	0.0086 m/sec	0.4197	7.0739	239.3	5941.0

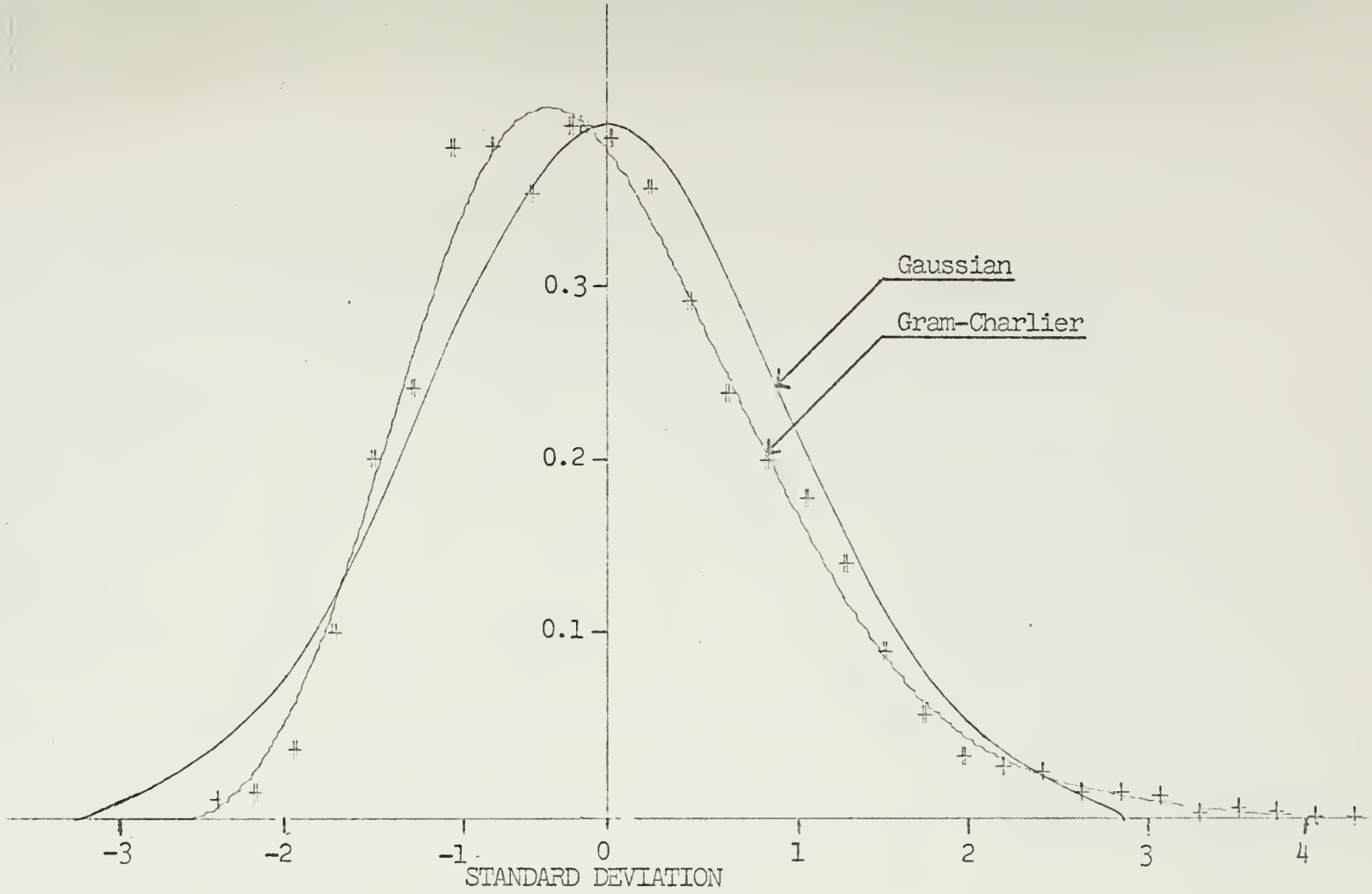

FIGURE 9. Frequency Distribution of Wave Pressure at Seaward Station Plotted with Gaussian and Gram-Charlier Distributions

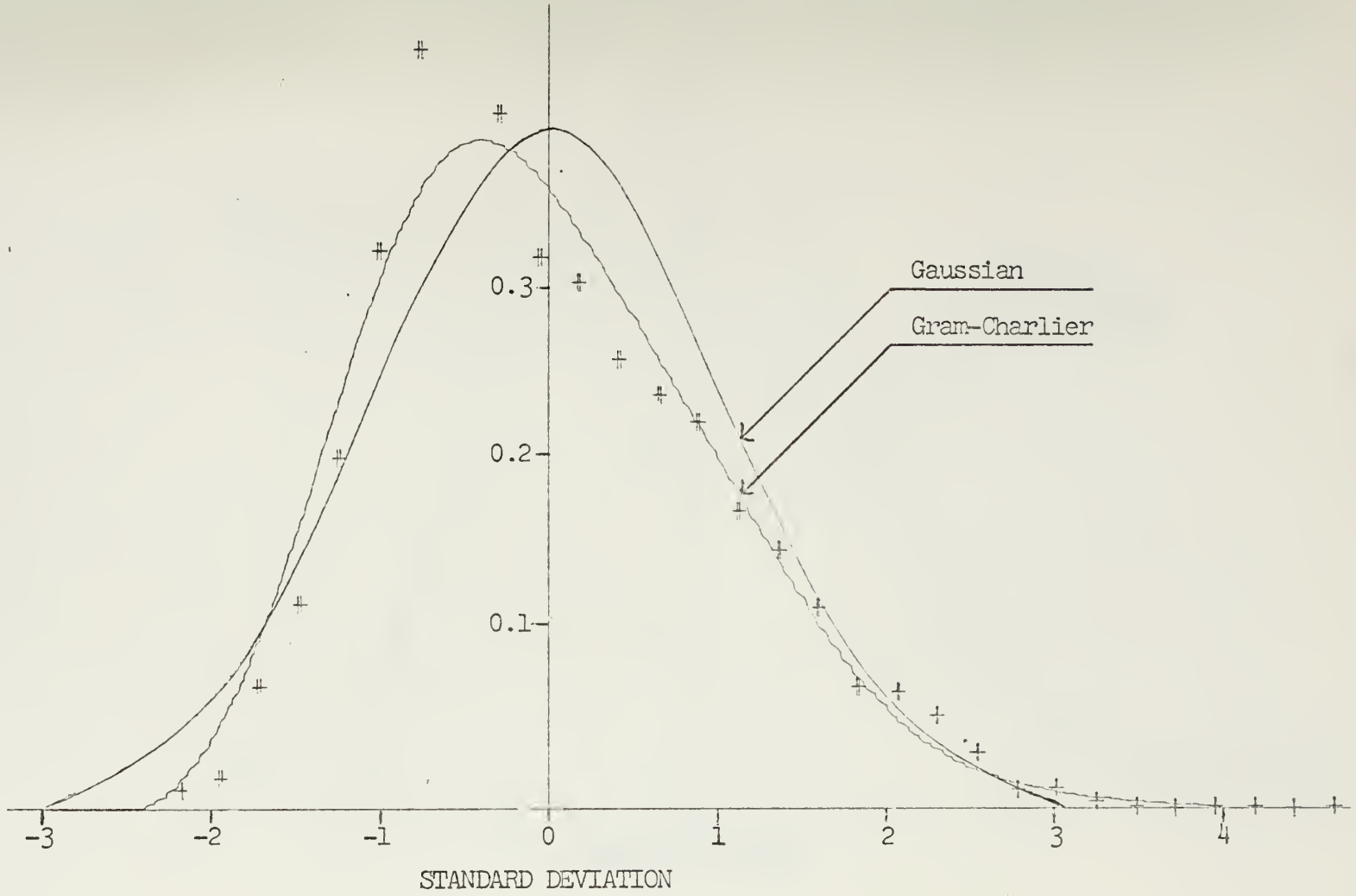

FIGURE 10. Frequency Distribution of Wave Pressure at Main Tower Plotted with Gaussian and Gram-Charlier Distributions

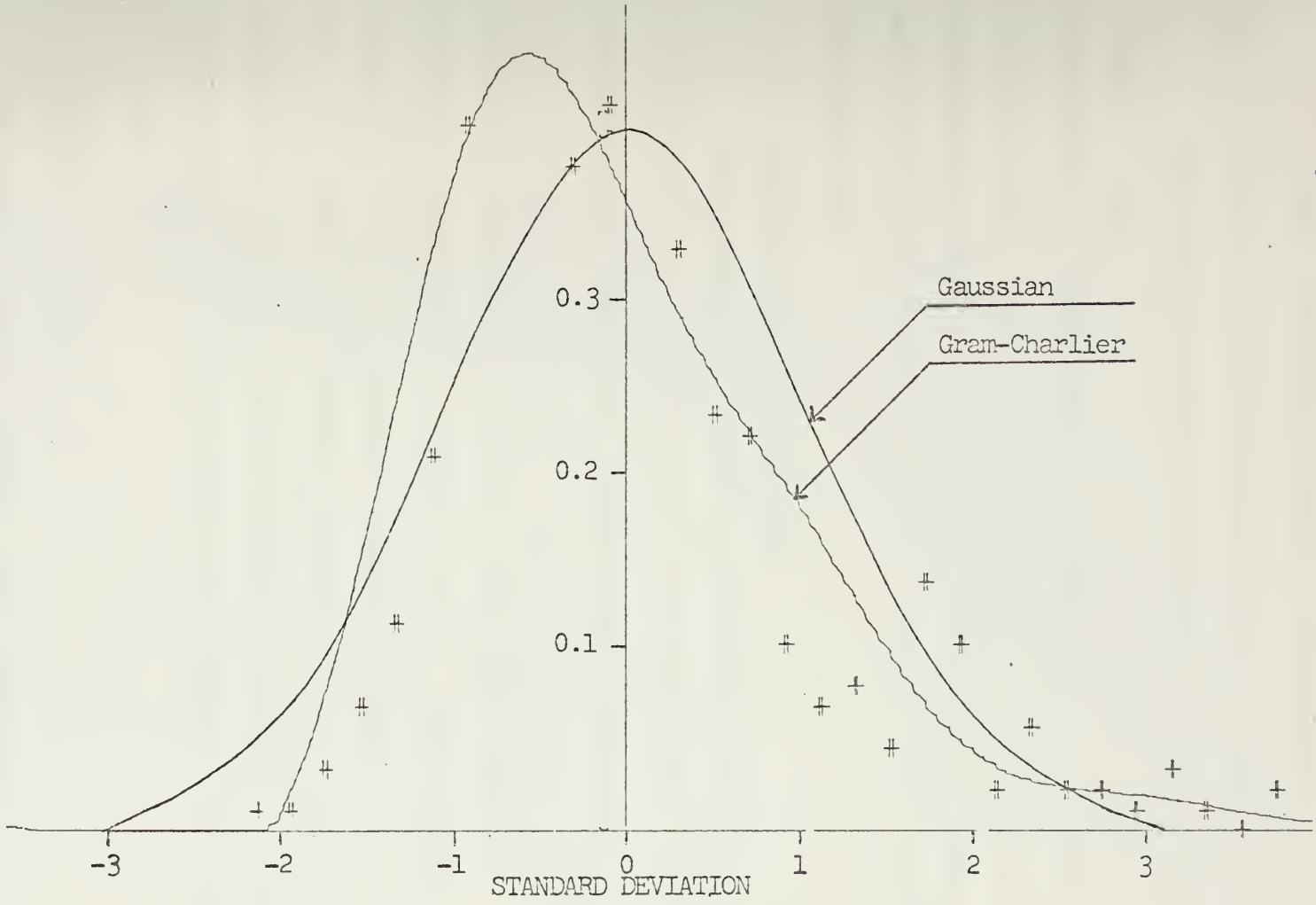

FIGURE 11. Frequency Distribution of Wave Height Measured with Capacitance Wave Gauge Plotted with Gaussian and Gram-Charlier Distributions

At the shoreward station, the distribution again more closely resembles the Gram-Charlier [Figure (12)].

The positive skewness measured at each station indicates a large number of small negative values and a higher probability of large positive values of wave height and velocity when compared to the Gaussian. This qualitative observation supports the notion that in shallow water, the wave crests are steep and narrow, and the wave troughs are flat and wide.

2. Water Particle Velocity

The probability density functions shown in Figures (13) and (14) for water particle velocity again follow the Gram-Charlier distribution more closely than they do the Gaussian. The Gram-Charlier distribution was computed by carrying the series to include the fourth moments of the frequency distribution (Equation 2.3). This appeared to be sufficient at the seaward station [Figure (9)]. However, due to the more non-linear situation in the surf zone, it appears that higher moments should be included. This would give a better fit and get rid of the humps in the tails of the distribution.

C. SPECTRAL ANALYSIS

The energy-density spectrum was calculated for each of the data records. Cross-spectra were then computed between variables, from which the coherence and phase were determined. Wave energy-density spectral components were computed from

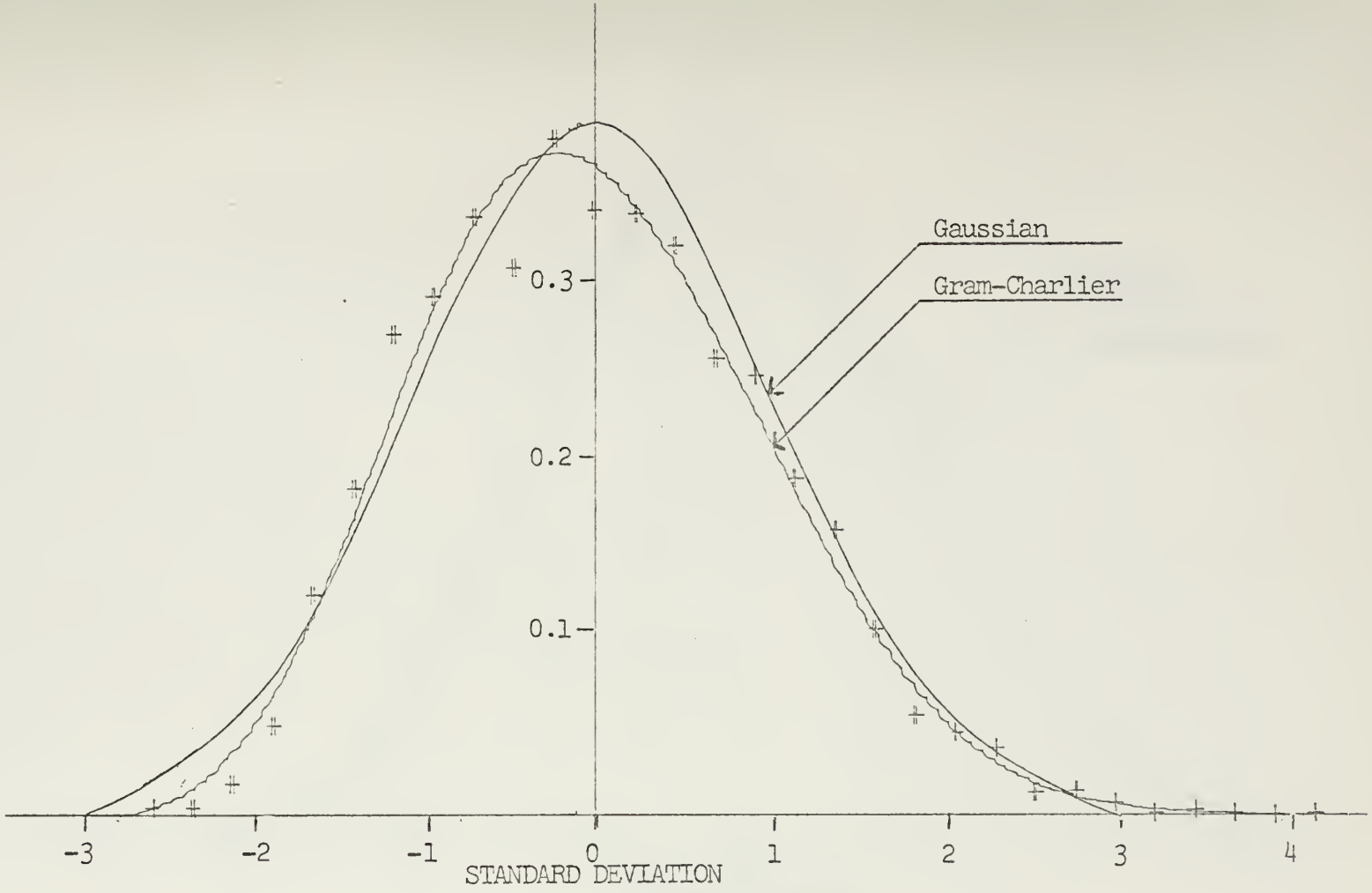

FIGURE 12. Frequency Distribution of Wave Height Measured with Baylor Wave Gauge Plotted with Gaussian and Gram-Charlier Distributions

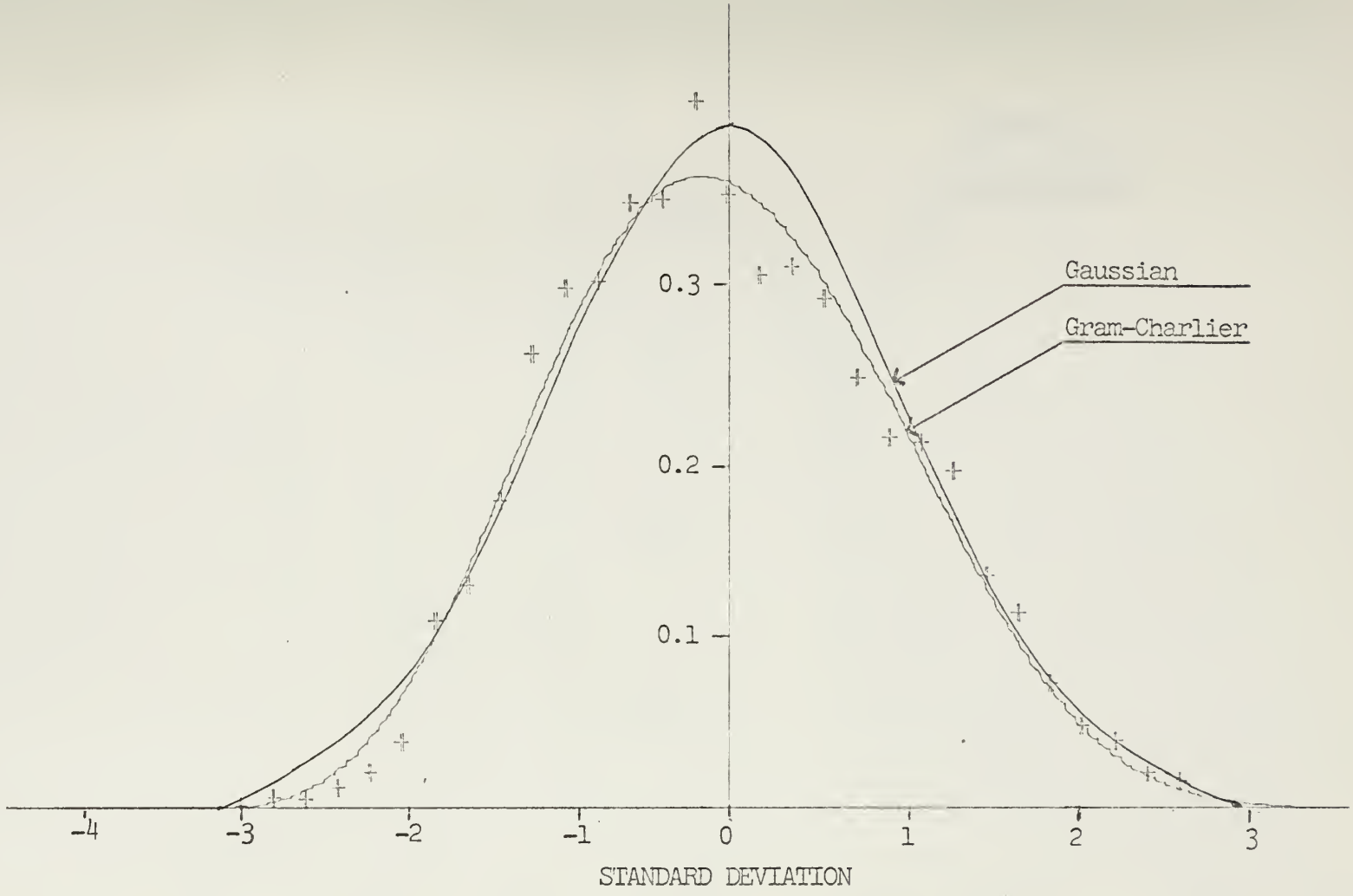

FIGURE 13. Frequency Distribution of Horizontal Water Particle Velocity Plotted with Gaussian and Gram-Charlier Distributions

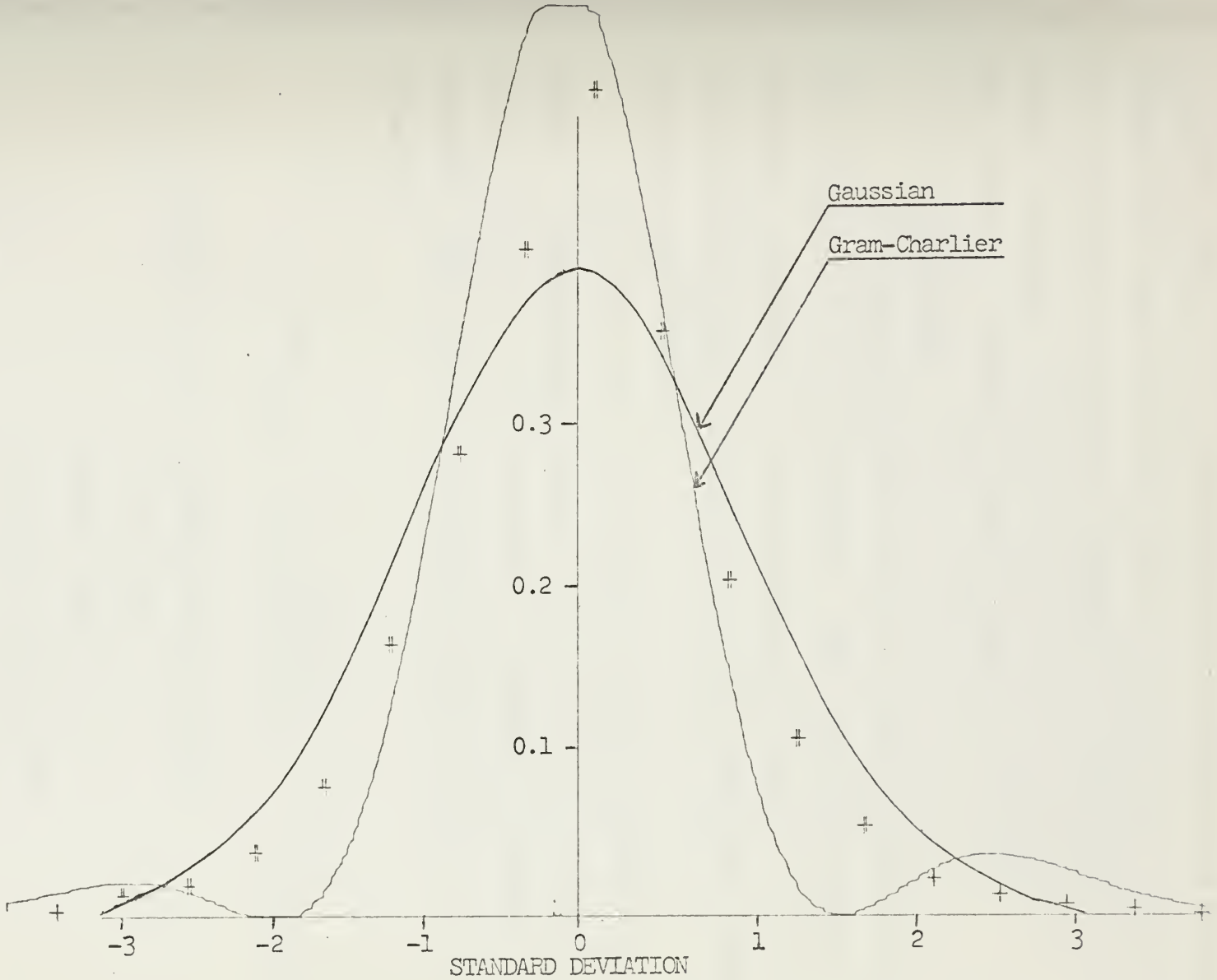

FIGURE 14 Frequency Distribution of Vertical Water Particle Velocity Plotted with Gaussian and Gram-Charlier Distributions

pressure energy-density components using linear wave theory. Linear wave theory was also used to transform the wave spectral components to spectral estimates of horizontal and vertical velocities. These calculated spectral values were then compared to measured particle velocity spectra.

1. Wave Height

The capacitance wave gauge was taken as the primary wave height measuring instrument. The capacitance gauge gave a direct measurement of instantaneous sea surface elevation, and by taking the mean, a measure of the average sea surface elevation was obtained.

The waves were also measured using a pressure wave gauge. To spectrally convert these pressure fluctuations to values of water surface elevation, a transfer function was applied. This function is based on linear theory, and is given as:

$$S(f)_{(wave)} = \left[\frac{\cosh kh}{\rho g \cosh k(h+z)}\right]^2 S(f)_{(pressure)} \qquad (4.1)$$

where: $S(f)$ = energy-density spectra

k = wave number

h = water depth

z = pressure sensor depth

The energy-density spectra of both the capacitance and pressure wave gauges are shown in Figure (15). The pressure spectrum has been converted to a wave spectrum

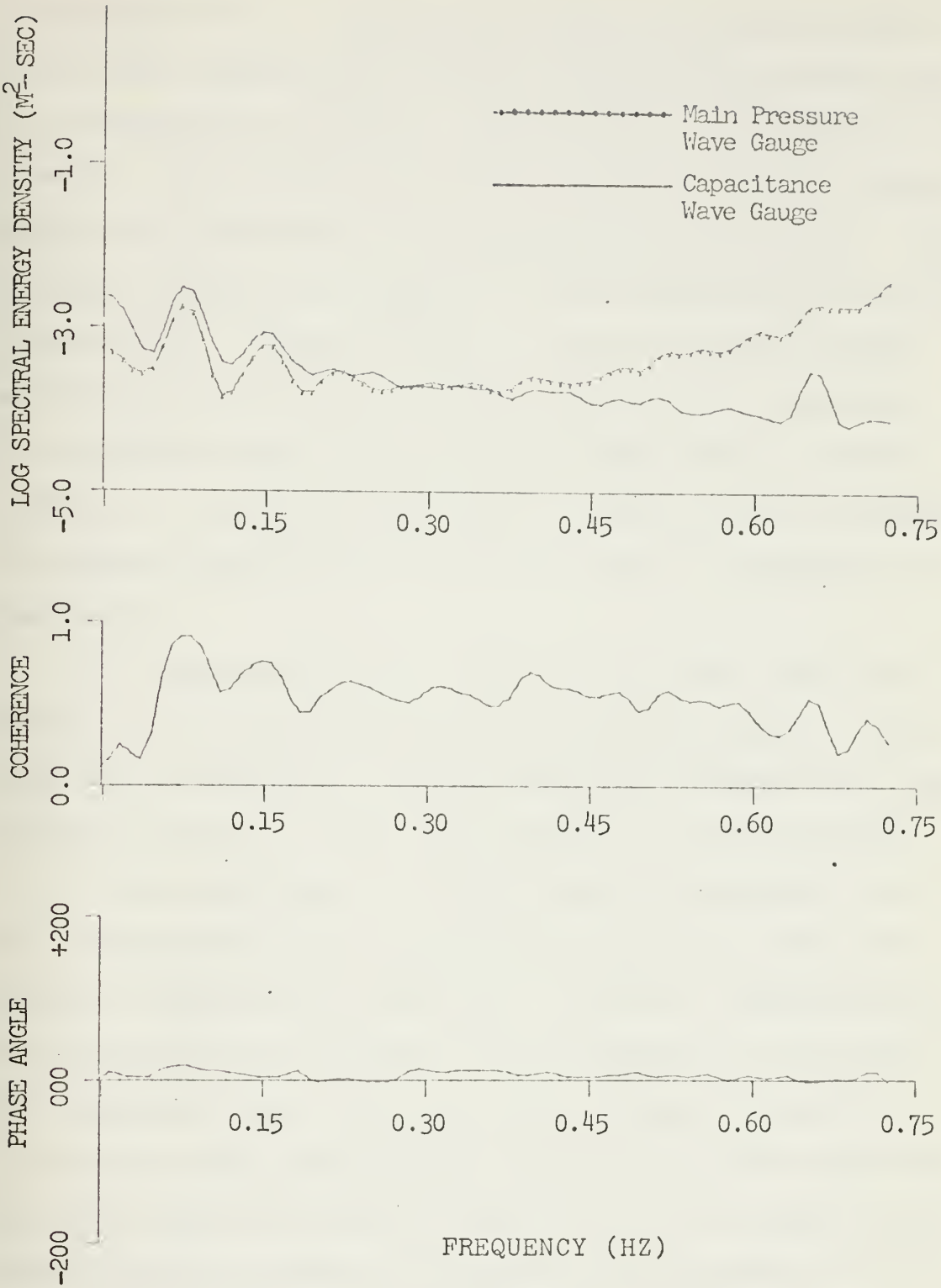

FIGURE 15. Spectra of Wave Height Comparing Main Pressure Wave Gauge and Capacitance Wave Gauge

using Equation 4.1. The spectra, which are characteristic of all the records, show a narrow banded energy-density peak at a frequency of 0.07 Hz., corresponding to a period of 14.3 seconds. Also evident are peaks at 0.14 and 0.21 Hz. which appear to be harmonics of the primary peak at 0.07 Hz. These harmonics appear to be physical as was observed from the strip chart earlier. These harmonics probably also have energy contributions due to the Fourier computational technique. A low frequency peak is also shown at about 0.02 Hz. corresponding to a period of 50 seconds. Energy at this frequency is commonly measured along this coast and is attributed to surf beat.

A peak occurs in all spectra at 0.6 Hz. This is attributed to mechanical noise in the tape recorder. This peak is at a frequency outside the range of appreciable wave energy and does not affect the results of the experiment.

The magnitude of the wave spectral components at the frequency of peak energy density calculated from the pressure record using linear wave theory was approximately 60 percent of that measured by the capacitance wave gauge. The coherence values were very high, ranging to greater then 0.9 in the maximum energy portion of the wave spectrum. The phase spectrum shows the capacitance wave gauge measurements generally leading the pressure measurements by a few degrees, probably due to the ability of the capacitance gauge to better measure the curling portion of the wave.

The spectra of the offshore wave gauge and the capacitance wave gauge were compared, as were the inshore and capacitance gauges [Figures (16) and (17)]. A dynamic pressure correction [Equation 4.1] was not applied to the seaward pressure gauge. The results show that the waves were shoaling throughout the process; that is, there was a gradual buildup of energy as the wave progressed from outside the breaker zone into the breaker zone.

The greater variance at the inshore wave gauge compared with the wave gauge at the breaker line is attributed to energy reflection from the beach. The Baylor wave gauge tower was approximately 25 meters from the point at which mean water level intersects with the beach, and 12.5 meters shoreward of the mean breaker line where the flow meter and primary wave gauges were located. These distances correspond to one-half and one-quarter wave lengths, respectively, of a 13 second period progressive wave in a depth of 1.9 meters. This arrangement places a node at the breaker line and an anti-node at the Baylor wave gauge tower for a standing wave of this period. This 13 second period corresponds closely to the period of peak energy.

The phase for a theoretical progressive wave is plotted with the measured phase for comparison in Figure (17). The phase relationship was calculated using linear wave theory. Deviations from the calculated progressive phase angle could be attributed to wave reflections.

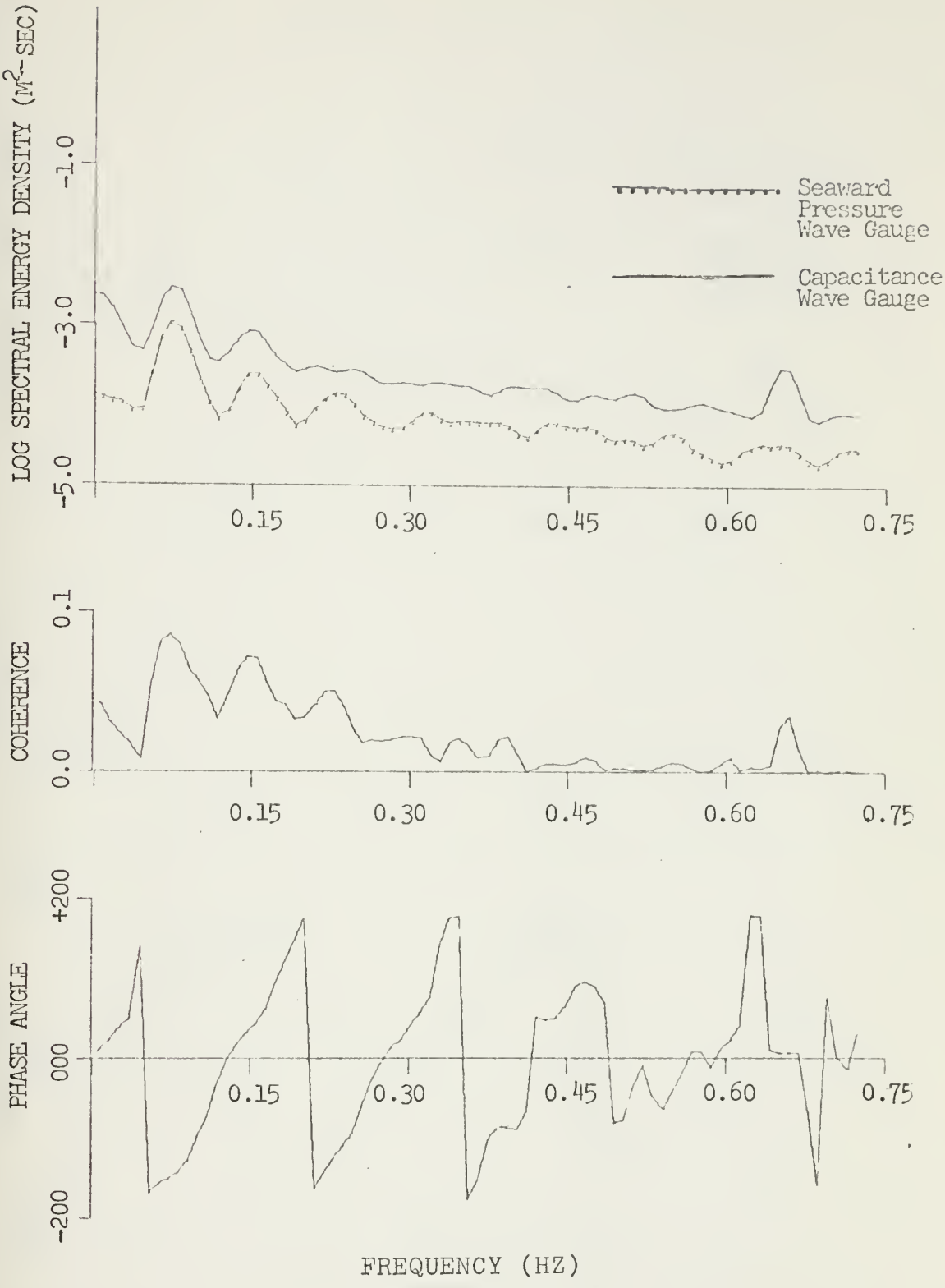

FIGURE 16. Spectra of Wave Height Comparing Seaward Pressure Wave Gauge and Capacitance Wave Gauge

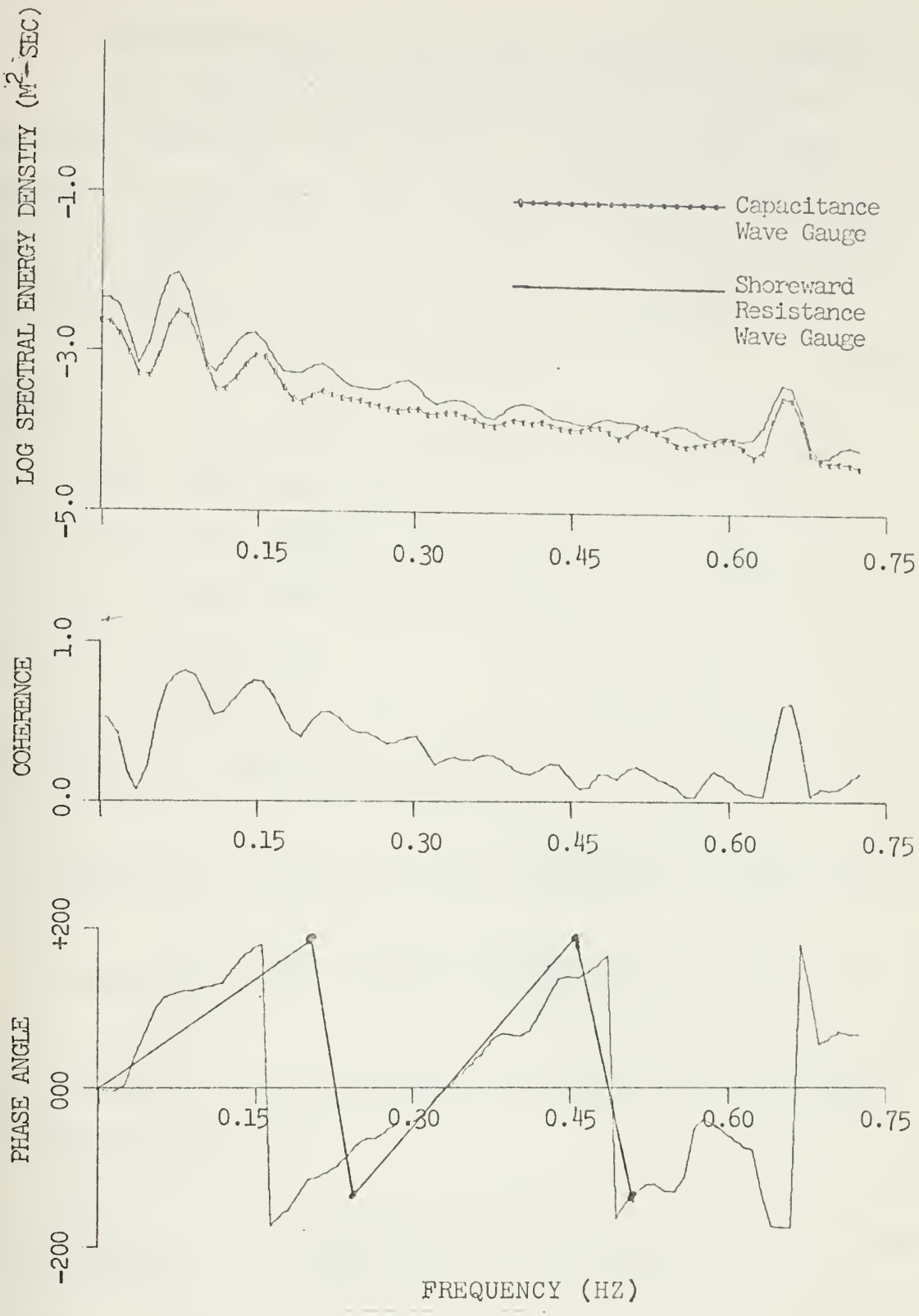

FIGURE 17. Spectra of Wave Height Comparing Shoreward Resistance (Baylor) Wave Gauge and Capacitance Wave Gauge

2. Sea Surface Elevation and Water Particle Velocity

The spectra of sea surface elevation and water particle velocities were compared by using linear wave theory to convert from wave spectral components to water particle velocity spectral components. The water surface elevation described by linear theory is given by:

$$\eta = a \cos (kx - \sigma t) \tag{4.2}$$

where

η = sea surface elevation

a = wave amplitude

k = wave number

x = horizontal cartesian coordinate

σ = frequency

t = time

The velocity components are given by:

$$\text{Horizontal velocity} = u = a\sigma \frac{\cosh k(h+z)}{\sinh kh} \cos(kx - \sigma t) \tag{4.3}$$

$$\text{Vertical velocity} = w = a\sigma \frac{\sinh k(h+z)}{\sinh kh} \sin(kx - \sigma t) \tag{4.4}$$

The horizontal velocity spectrum calculated from the wave spectrum is given by:

$$S(f)_{(vel)} = \left[\sigma \frac{\cosh k(h+z)}{\sinh kh}\right]^2 S(f)_{(wave)} \tag{4.5}$$

and the vertical velocity spectrum by:

$$S(f)_{(vel)} = [\sigma \frac{\sinh k(h+z)}{\sinh kh}]^2 S(f)_{(wave)} \qquad (4.6)$$

where the terms in brackets are the corresponding transfer functions.

a. Horizontal Water Particle Velocity

Linear theory under-calculates the horizontal velocity spectrum by 50 percent at the peak energy point [See Figure (18)]. The values of coherence are high, ranging above 0.75. The phase angle, which according to linear theory should equal zero, ranges up to 43 degrees from its average value of about 20 degrees. This shows the crest of the unstable breaking wave leading the horizontal particle velocities in the body of the flow. This compares well with the laboratory findings by Adeyemo (1970) that the maximum shoreward horizontal velocity for monochromatic waves occurs 25 degrees after the passage of the wave crest.

b. Vertical Water Particle Velocity

The measured rms vertical velocity was an order of magnitude less than the measured rms horizontal velocity, and showed very little wave induced motion [Figure (19)]. The coherence reached a maximum value of 0.37 at a frequency of 0.15 Hz., which is above the frequency of maximum energy as measured for the wave and horizontal velocity spectra. A phase angle of 130° to 145° was computed, in contrast to the theoretical value of 90° between wave height and vertical velocity.

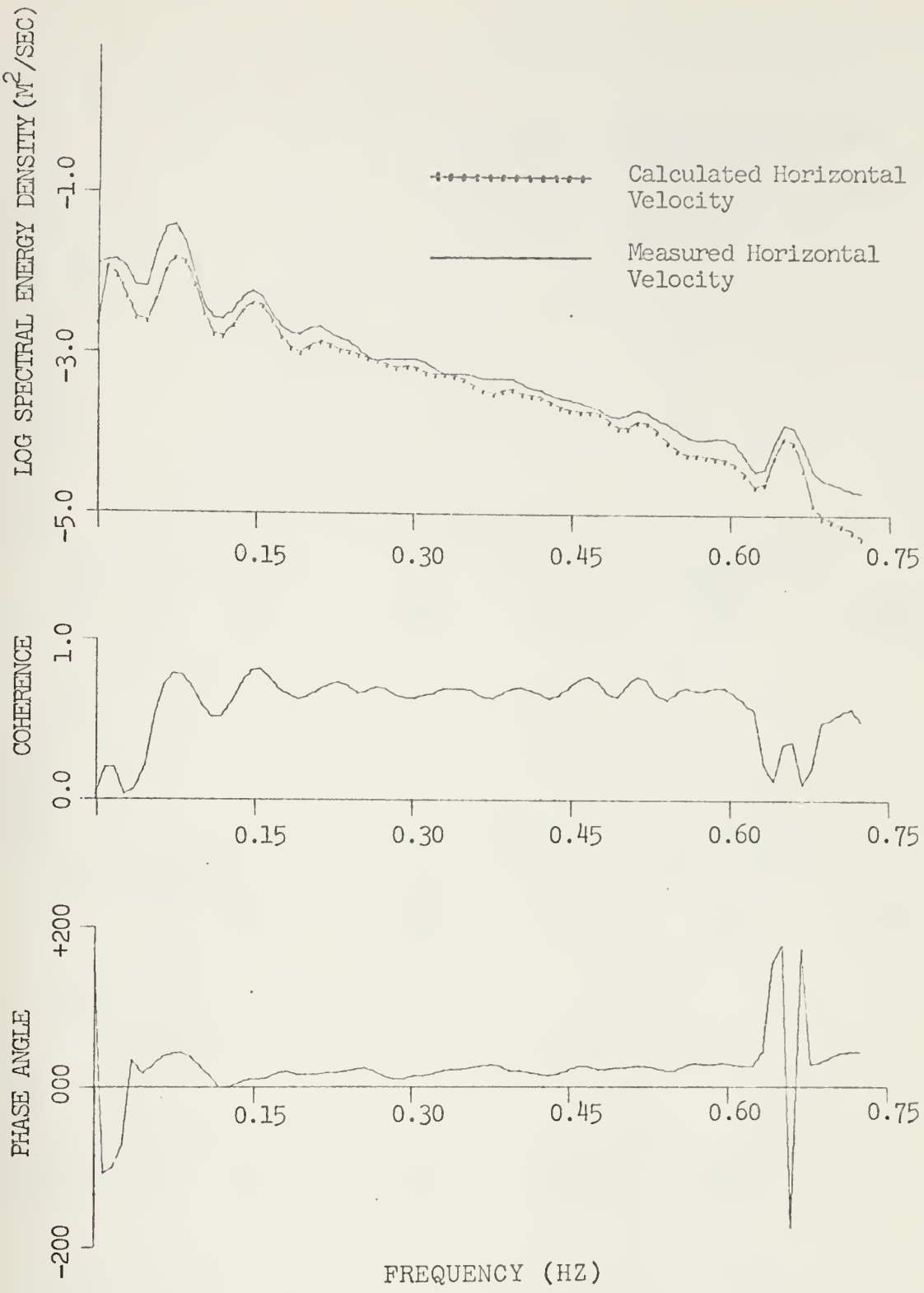

FIGURE 18. Spectra of Measured and Calculated Horizontal Velocity

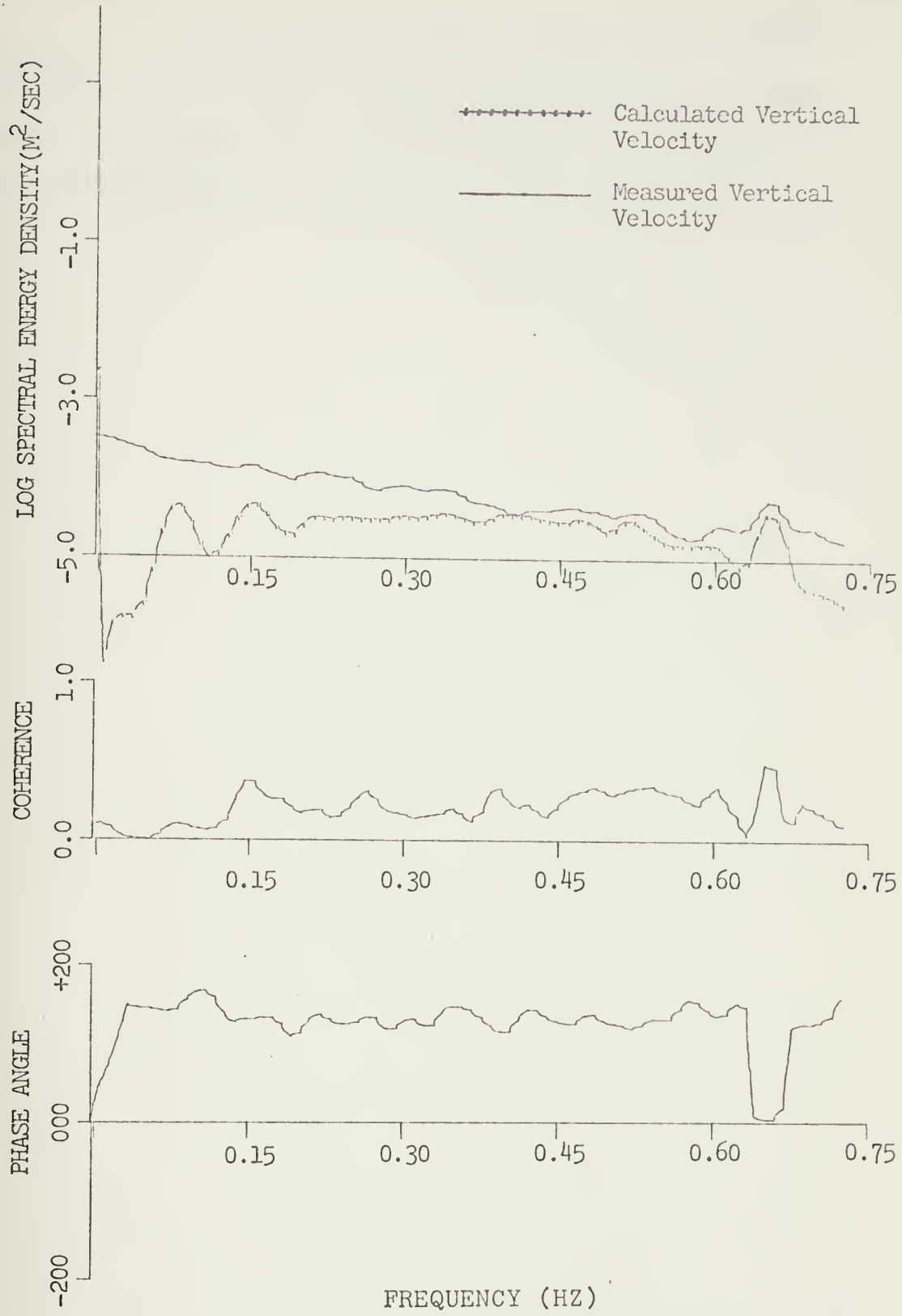

FIGURE 19. Spectra of Measured and Calculated Vertical Velocity

The lack of coherence between water surface elevation and vertical velocity could be due to a noisy electrical signal from the instrument, a conversion of wave-induced motion to turbulent motion, or both.

V. CONCLUSIONS

The probability density functions for the various records compared better with the Gram-Charlier distribution than with the Gaussian distribution when tested using the chi-square goodness-of-fit test. This result verifies the observed asymmetrical shape of the waves in the breaker zone and points out the importance of including higher order moments in describing wave phenomena in very shallow water.

The values of the horizontal velocity energy-density spectral components calculated from wave spectra using linear theory indicate a qualitative, but not a quantitative relationship. In general, linear theory underpredicts the magnitude of the velocity spectra.

The high coherence between waves and horizontal velocity shows that most of the motion in the body of the breaking wave is wave-induced. A similar conclusion could not be drawn when comparing waves and vertical velocity.

The spectral difference between water surface elevation and horizontal velocity was near that predicted by linear theory. The waves lead the horizontal velocity in spectral phase on the average by 20 degrees, implying that the "curling" crest of the wave arrives prior to maximum water particle velocity.

In summary, the water particle motion in the breaking waves seems to be very much wave induced in the body of the

flow. Linear theory under-predicts the magnitude of the velocity spectra when computing from wave spectra.

BIBLIOGRAPHY

1. Adeyemo, M. D., Velocity Fields in the Wave Breaker Zone, Proceedings of the Twelth Coastal Engineering Conference, ASCE, 1970.

2. Bendat, J. S., and Piersol, A. G., Measurement and Analysis of Random Data, John Wiley and Sons, Inc., New York, 1966.

3. Blackman, R. B., and Tukey, J. W., The Measurement of Power Spectra, Dover Publications, Inc., New York, 1958.

4. Collins, J. I., Probabilities of Breaking Wave Characteristics, Proceedings of the Twelth Coastal Engineering Conference, ASCE, 1970.

5. Inman, D. L., and Nasu, N., Orbital Velocity Associated With Wave Action Near the Breaker Zone, U. S. Army Corps of Engineers, Beach Erosion Board, Technical Memorandum No. 79, March, 1956.

6. Iversen, H. W., Waves and Breakers in Shoaling Water, Proceedings of the Third Conference on Coastal Engineering, Council on Wave Research, 1953.

7. Krapohl, R. F., Wave-Induced Water Particle Motion Measurements, M. S. Thesis, U. S. Naval Postgraduate School, Monterey, California, 1972.

8. McGoldrick, L. F., A System for the Generation and Measurement of Capillary-Gravity Waves, Department of the Geophysical Sciences, University of Chicago, Technical Report No. 3, August, 1969.

9. Miller, R. L., and Zeigler, J. M., The Internal Velocity Fields in Breaking Waves, Proceedings of the Ninth Conference on Coastal Engineering, ASCE, 1964.

10. Steer, R., Kinematics of Water Particle Motion Within the Surf Zone, M. S. Thesis, U. S. Naval Postgraduate School, Monterey, California, 1972.

11. Thornton, E. B., A Field Investigation of Sand Transport in the Surf Zone, Proceedings of the Eleventh Conference on Coastal Engineering, ASCE, 1969.

12. Walker, J. R., Estimation of Ocean Wave-Induced Particle Velocities from the Time History of a Bottom Mounted Pressure Transducer, M. S. Thesis, University of Hawaii, 1969.

INITIAL DISTRIBUTION LIST

		No. Copies
1.	Defense Documentation Center Cameron Station Alexandria, Virginia 22314	2
2.	Library, Code 0212 Naval Postgraduate School Monterey, California 93940	2
3.	Dr. Edward B. Thornton Department of Oceanography Naval Postgraduate School Monterey, California 93940	5
4.	LCDR David P. Richardson General Delivery Carmel, California 93921	5
5.	Department of Oceanography Naval Postgraduate School Monterey, California 93940	3
6.	Oceanographer of the Navy Hoffman Building No. 2 2461 Eisenhower Avenue Alexandria, Virginia 22314	1
7.	Office of Naval Research Department of the Navy Code 480 Arlington, Virginia 22217	1
8.	Dr. Robert E. Stevenson Scientific Liaison Office Scripps Institution of Oceanography La Jolla, California 92037	1
9.	Associate Professor Jacob B. Wickham Oceanography Department Naval Postgraduate School Monterey, California 93940	1
10.	Dr. D. L. Harris Coastal Engineering Research Center Corps of Engineers, U. S. Army 5201 Little Falls Road, N. W. Washington, D. C. 20315	1

11. Director 1
Coastal Engineering Research Center
Corps of Engineers, U. S. Army
5201 Little Falls Road, N. W.
Washington, D. C. 20315

12. Chief of Naval Research 1
Geography Branch, Code 414
Office of Naval Research
Washington, D. C. 20360

13. Dr. Jacob Van De Kreeke 1
School of Marine and Atmospheric Sciences
Division of Ocean Engineering
10 Rickenbacker Causeway
Miami, Florida 33149

14. Dr. Warren C. Thompson 1
Oceanography Department
Naval Postgraduate School
Monterey, California 93940

SECURITY CLASSIFICATION OF THIS PAGE (When Data Entered)

REPORT DOCUMENTATION PAGE		READ INSTRUCTIONS BEFORE COMPLETING FORM
1. REPORT NUMBER	2. GOVT ACCESSION NO.	3. RECIPIENT'S CATALOG NUMBER
4. TITLE (and Subtitle) The Kinematics of Water Particle Velocities of Breaking Waves Within the Surf Zone		5. TYPE OF REPORT & PERIOD COVERED Master's Thesis; September 1973 6. PERFORMING ORG. REPORT NUMBER
7. AUTHOR(s) David Paul Richardson		8. CONTRACT OR GRANT NUMBER(s)
9. PERFORMING ORGANIZATION NAME AND ADDRESS Naval Postgraduate School Monterey, California 93940		10. PROGRAM ELEMENT, PROJECT, TASK AREA & WORK UNIT NUMBERS
11. CONTROLLING OFFICE NAME AND ADDRESS Naval Postgraduate School Monterey, California 93940		12. REPORT DATE September 1973 13. NUMBER OF PAGES 59
14. MONITORING AGENCY NAME & ADDRESS(if different from Controlling Office) Naval Postgraduate School Monterey, California 93940		15. SECURITY CLASS. (of this report) Unclassified 15a. DECLASSIFICATION/DOWNGRADING SCHEDULE

16. DISTRIBUTION STATEMENT (of this Report)

Approved for public release; distribution unlimited.

17. DISTRIBUTION STATEMENT (of the abstract entered in Block 20, if different from Report)

18. SUPPLEMENTARY NOTES

19. KEY WORDS (Continue on reverse side if necessary and identify by block number)

Breaking Waves
Waves
Surf Zone

20. ABSTRACT (Continue on reverse side if necessary and identify by block number)

Simultaneous measurements of waves, and vertical and horizontal water particle velocities were made at the breaker-line within the surf zone using a capacitance type penetrating wave staff, a pressure wave gauge, and an electromagnetic current meter. Wave measurements were also made at seaward and shoreward locations. The wave energy-density spectral components were converted to velocity spectral components using linear wave

DD FORM 1 JAN 73 1473 EDITION OF 1 NOV 65 IS OBSOLETE
S/N 0102-014-6601 |
(Page 1)

SECURITY CLASSIFICATION OF THIS PAGE (When Data Entered)

theory. These computed values compared well qualitatively with the measured velocity spectra. Quantitatively, the results showed that linear theory underpredicted wave-induced horizontal velocity spectral components by about 50 percent at the frequency of peak energy. The coherence values between waves and horizontal velocity were high, ranging above 0.75. The phase angle computation showed the calculated velocity components leading the measured velocity components by an average of 20 degrees, indicating an unstable wave crest leading the particle motion in the body of the wave. Probability density functions were computed and compared to Gaussian and Gram-Charlier distributions using the chi-square goodness-of-fit test. The Gram-Charlier distribution qualitatively gave the better fit to the data.